SITE-SPECIFIC IMMOBILIZATION OF TETRAZINE-MODIFIED GREEN FLUORESCENT PROTEIN ON TRANS-CYCLOOCTENE SURFACES

by

Daniel K. Clark Jr.

A thesis submitted to the Faculty of the University of Delaware in partial fulfillment of the requirements for the degree of Master of Science in Chemistry and Biochemistry

Spring 2016

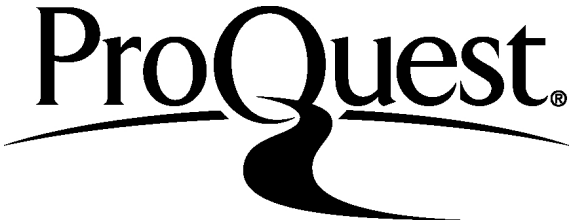

SITE-SPECIFIC IMMOBILIZATION OF

TETRAZINE-MODIFIED GREEN FLUORESCENT PROTEIN

ON TRANS-CYCLOOCTENE SURFACES

by

Daniel K. Clark Jr.

Approved: _____

Thomas P. Beebe Jr., Ph.D.
Professor in charge of thesis on behalf of the Advisory Committee

Approved: _____

Murray Johnston, Ph.D.
Chair of the Department of Chemistry and Biochemistry

Approved: _____

George H. Watson, Ph.D.
Dean of the College of College of Arts and Sciences

Approved: _____

Ann L. Ardis, Ph.D.
Senior Vice Provost for Graduate and Professional Education

ACKNOWLEDGMENTS

I would like to thank God, first and foremost, for opening the doors that needed to be opened which have allowed me the opportunity to pursue my passions and broaden my horizons within the chemistry community. I would also like to thank my research advisor Dr. Thomas P. Beebe, Jr. for his continued support, guidance, and opportunities in helping develop a direction that has and will always influence my outlook in life.

I would like to thank all the members of the Beebe Research Group, both past and present, for their assistance in contributing to my efforts in completing and being successful with my research endeavors. If it had not been for the continued support and encouragement of these colleagues, as well as other University of Delaware research group members, I do not think my journey would have been as gratifying as it has been.

I would like to thank my entire family, especially my children and parents, who have supported me in so many capacities in order to ensure I am successful in my endeavors. My journey in accomplishing this feat has come with many struggles and has involved many sacrifices, but given the opportunity again, I believe that I would repeat my choice and direction.

TABLE OF CONTENTS

LIST OF TABLES

LIST OF FIGURES

ABSTRACT

The ability to control the orientation of proteins attached to a surface, one of the goals of this work, has applications within areas such as microarrays, biomaterials, tissue engineering and biosensors. Non-covalent protein adsorption (physisorption), the easiest of all protein-attachment approaches, suffers from several drawbacks and was rejected for this work. Although the covalent attachment (chemisorption) of peptides and proteins to solid substrates has long been achieved, many of the procedures utilized are generally limited to schemes and reaction steps that can be detrimental to biological systems. Furthermore, while the attachment is covalent, the point(s) of attachment on the protein and its subsequent orientation at the surface remain uncontrolled, resulting in a distribution of protein orientations at the surface, and therefore a decrease in the effective bioactivity sought. The focus herein was to investigate the feasibility of control of attachment site(s) on the protein, and hence, the orientation of the protein at the surface. Specifically, we sought to functionalize a glass support substrate with one of several cyclooctene compounds (patterned through micro-contact printing, or un-patterned by simple immersion), followed by reaction in these functionalized areas with a site-specifically modified tetrazine-protein moiety, either through ‘click chemistry’ or non-specific binding (as a control for comparison purposes). While the strain-driven reactivity of cis- vs. trans-cyclooctene have been studied in homogenous solution systems, this is the first study of the reaction scheme at a surface. Time-of-flight secondary ion mass spectrometry (ToF-SIMS), fluorescence imaging, contact angle analysis, and principal component analysis were

utilized to determine the outcome of each step in the reaction scheme. The covalent attachment of tetrazine-modified protein with trans-cyclooctene-modified surfaces was observed, as expected, whereas only non-specific absorption was observed on the cis-cyclooctene-modified surfaces.

Chapter 1

INTRODUCTION

Adhering biomolecules on surfaces with patterning on the micron to nanometer scale has applications ranging from model systems to characterize protein-protein interactions, protein-small molecule interactions, to technologies that can improve the performance of biomedical implants.[1,2,3,4] Current techniques employed for the immobilization of biological molecules on surfaces are often limited to particular proteins, non-specific adsorption of a protein to the aqueous-solid interface, or covalent attachment of a protein at the aqueous-solid interface. However useful, there are considerable limitations to these immobilization techniques. Non-specific adsorption of a protein to a surface does not allow for control of the orientation of the protein, which can cause structural changes or denaturation, impacting responses between cells and the bound protein.[5,6,7,8] In covalent binding schemes, multiple binding sites are often utilized, leading to an uncontrolled distribution of protein orientations at the surface.[9,10] It is known that the type of biomolecule, its identity within a certain type, its orientation, its conformation, and its coverage all affect the interactions between a solid-phase platform and the cellular interface.[11] In order to evaluate efficiently the biological or cellular interface, the surface-bound protein will need to have a controlled orientation and retain its native structure.[12,13,14]

In this work, we offer a cost-effective and simple method to develop functionalized micron-scale patterns on glass surfaces, while also controlling the orientation of a bound biomolecule. Our initial test system consisted of tetrazine-

modified green fluorescent protein (GFP). Glass surfaces that were patterned with trans-cyclooctene allow for a rapid biorthogonal ligation with the site-specifically modified tetrazine-protein.[15,16,17,18] As a non-reactive control for non-specific physisorption, cis-cyclooctene patterned surfaces were employed. By utilizing ToF-SIMS, fluorescence microscopy, and principal component analysis, the differences in bound proteins were evaluated.

1.1 Time-of-Flight Secondary Ion Mass Spectrometry (ToF-SIMS)

In order to obtain the molecular information about the surface of the functionalized glass surfaces, ToF-SIMS was utilized (Figure 1.1). ToF-SIMS is an instrumental technique that allows the desorption and detection of ionized molecular material (all elements, including hydrogen) from the first 1-3 nm of a surface being analyzed.[19,20] The instrument utilizes a pulsed primary-ion beam to bombard a sample surface and generate both charged and neutral secondary species derived from the sample surface (Figure 1.2). The emitted, charged secondary ions are focused into a reflectron-type time-of-flight mass analyzer, where they are allowed to separate based upon their mass-to-charge ratio *m/z* and hence flight time to the detector. The technique is able to provide elemental and molecular information with a mass resolving power ("mass resolution") up to $m/\Delta m$ = 10,000. Such high mass resolution allows for ions with the same nominal mass to be clearly distinguished and resolved from each other (e.g., Si^+, AlH^+, CO^+, N_2^+, and $C_2H_4^+$, all at the nominal mass of 28).[21] In addition to this, the primary-ion source, a liquid-metal ion gun (LMIG) can be focused into a beam with a sub-micrometer spot size, allowing high-lateral-resolution images in which ion intensity forms the image's contrast signal. Furthermore,

sensitivity is very good, providing the ability to detect compounds present at the parts-per-million to parts-per-billion range under many conditions.[22,23]

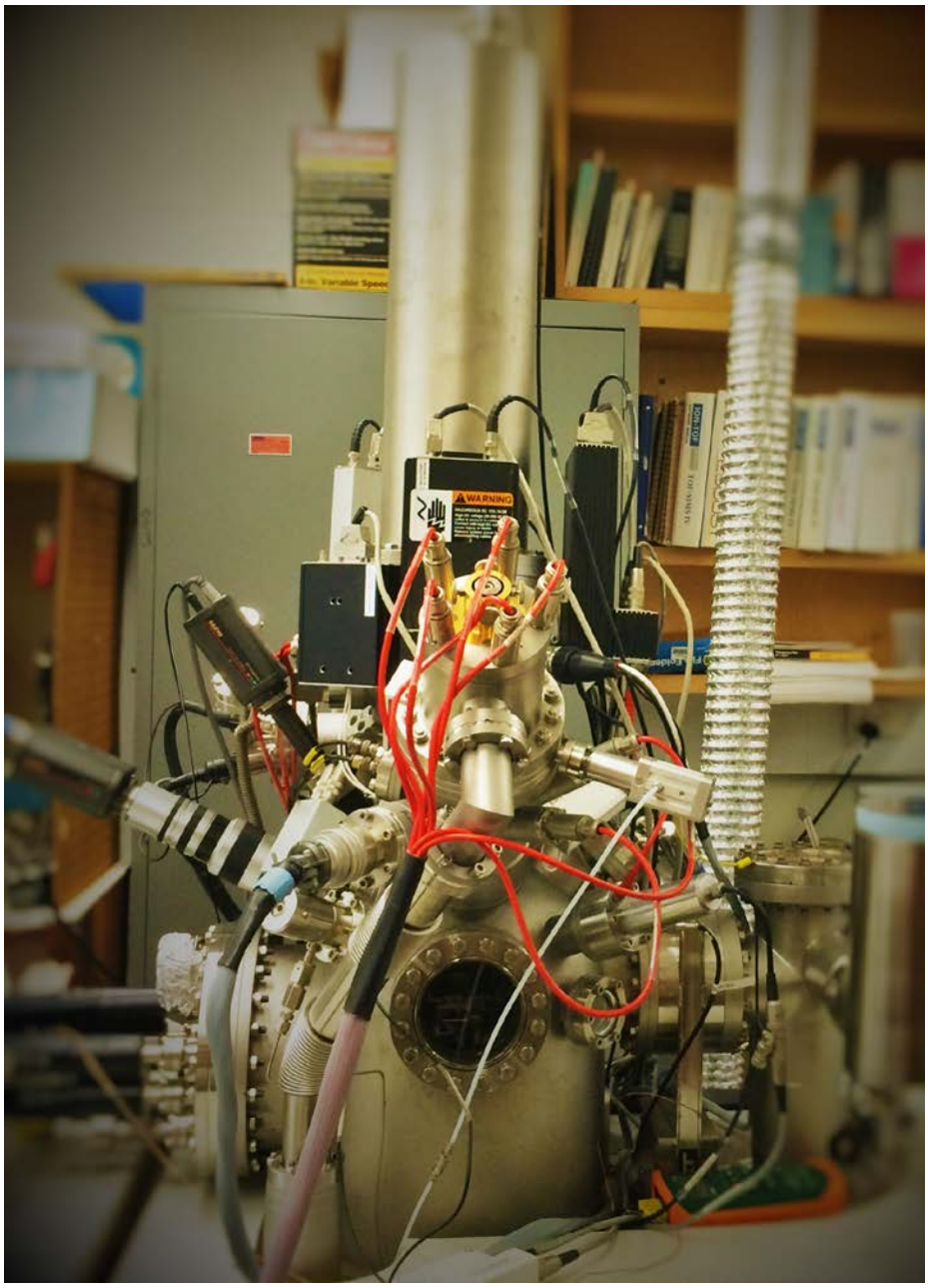

Figure 1.1. Photograph of the ToF-SIMS instrument that is located within the Surface Analysis Facility at the University of Delaware in Newark, DE, and used for the bulk of this work. (*Image courtesy of https://sites.udel.edu/saf/files/2014/10/tof-sims-2m7m0sf.jpg*)

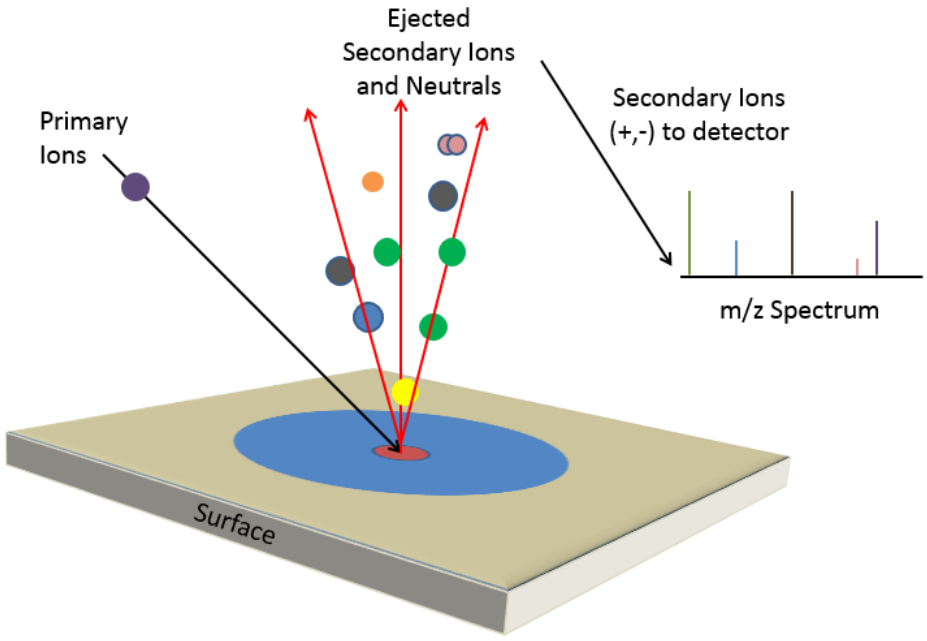

Figure 1.2 ToF-SIMS Schematic. A pulsed, focused primary ion beam is used to bombard the sample surface, causing the emission of neutral and charged secondary fragments. The charged secondary ions are directed to the mass analyzer where a *m/z* spectrum is generated, plotted as ion intensity vs. *m/z*.

In the broadest sense, ToF-SIMS is capable of collecting mass spectral data in two different modes: static or dynamic. Because of the energy that is imparted to the surface upon collision with a primary ion as part of the analysis, ion-induced damage can result and the surface's structure can be changed during analysis. Because of the possibility of ion-induced sample damage during secondary-ion formation, compounded with ToF-SIMS's high sensitivity, it is important that the analysis area only be sampled once so that secondary ions generated are consistent with the actual chemical composition of the surface, and not a surface damaged by analysis.

In static SIMS, which was utilized for the experimentation contained herein, less than 0.1% of the surface area within an analysis area is impacted and potentially damaged by the primary ion used to generate the secondary ions, leading to the term "static," and implying that the analysis process has not changed the sample surface. The generally accepted primary ion dose density for static SIMS analysis is less than 1×10^{12} ions cm^{-2}.[24] This figure is based on the fact that a single crystal metal surface contains on the order of 1×10^{15} atoms cm^{-2}. Therefore, when operating below the static SIMS limit, one can be sure that less than one in 1,000 surface atoms (or 0.1%) have been hit and possibly damaged by a primary ion. Depending on the type of primary ion used (e.g., Ar^+, Cs^+, SF_5^+, Ga^+, Au^+, Au_2^+, Au_3^+, Bi^+, Bi_2^+, Bi_3^+, C_{60}^+, Ar_{2000}^+), and the nature of the sample, the damaged area surrounding a single ion impact can have a diameter in the 1-nm to 100-nm range. To ensure that less than 0.1% of the surface area is impacted by a primary ion during a static SIMS analysis, the primary-ion dose density is kept low.

In the other analysis mode, dynamic SIMS, ion-induced sample "damage" is used to sputter into and remove layers of the sample during analysis, so as to

determine concentrations as a function of sample depth. Because of the aggressive nature of ion-induced sample removal, also known as sputtering, dynamic SIMS is limited to elemental analysis because molecular structure is damaged by the sputtering process. Dynamic SIMS was not used in the bulk of this work and will not be discussed further.

ToF-SIMS was used in the static mode in this experimental work to understand and verify that surface modifications had taken place at each reaction step. Due to the fact that static ToF-SIMS has high mass resolution and is both sensitive and surface-sensitive, it is an ideal instrumental technique for the analysis of surface-bound proteins.[25,26] The imaging capabilities of the instrumentation were also utilized to compare the localized chemistry created by micro-contact printing of patterned regions on the length scale of 40 to 80 micrometers. ToF-SIMS images were used here to quantify image contrast of laterally adjacent surface-functionalized regions, and to verify the successful modification of the surfaces.

1.2 Chemometrics

Multivariate analytical techniques are well established and widely used in the analytical community to identify important trends within large and complex data sets. One technique, principal component analysis (PCA) is used to reduce the dimensionality of ToF-SIMS and other data and identify useful information from less-useful, random noise. The process by which PCA is utilized to analyze ToF-SIMS spectra results in the formation of a *scores matrix* and a *loadings matrix* from the original data sets. The scores matrix for ToF-SIMS data are representative of the samples (each sample is a single mass spectrum) while the loadings matrix represents the variables in each mass spectrum (each variable is a peak intensity at a single *m*/*z*

value). Essentially, a new coordinate system is constructed from the original variables so that the first axis (Figure 1.3) contains the greatest variation between spectra. Each subsequent axis is orthogonal to the previous and accounts for the next-greatest variation between spectra.

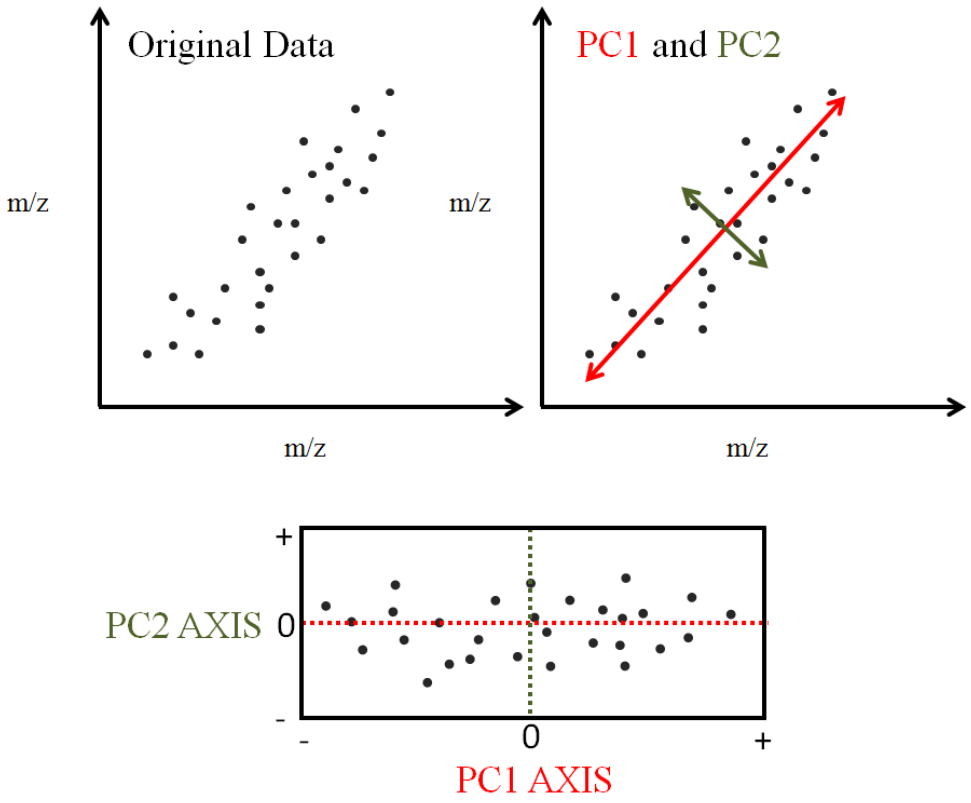

Figure 1.3 2-dimensional representation of original data and a new coordinate system based on orthogonal principal components.

Each of the generated orthogonal axes is called a principal component (PC) and is used to identify relationships between variables and samples. In the case of ToF-SIMS spectral data consisting of peak intensities at various *m/z* values, the peak

intensities at their respective *m/z* values are considered the variables. The intensities are different for different samples, and the PCA analysis seeks to identify the variance between these variables and link them back to the sample from which they were generated.

In more mathematical terms, PCA is implemented by determining the eigenvectors and eigenvalues of a covariance matrix. The covariance matrix is a measurement of how the change in one variable is associated with the change in another variable. The covariance matrix $\boldsymbol{S}$ of a data set $\boldsymbol{X}$ with *m*-rows (samples) and *n*- columns (peaks) is shown in Eq. 1.1:

$$S = cov(X) = (\frac{1}{m-1})X^T X \qquad \text{Equation 1.1}$$

where $\boldsymbol{S}$ is the covariance matrix and $\boldsymbol{X^T}$ is the transpose of $\boldsymbol{X}$. The covariance matrix is a matrix $\boldsymbol{X}$ that has elements evaluated by $X_{i,j} = cov(i,j)$. The sign of each numerical value (positive or negative) in the covariance matrix signifies that those variables are colinear. For example, if the numerical value in the covariance matrix is positive then as the *j* variable in data set $\boldsymbol{X}$ increased, so did the *i* variable. Values in the covariance matrix that are near or equal to zero have little or no correlation with each other and hence are independent. Eigenvalues and eigenvectors are then calculated via singular value decomposition of the covariance matrix. This reduces the original data matrix $\boldsymbol{X}$ into the sum of a cross-product of two smaller matrices $\boldsymbol{P}$ and $\boldsymbol{T}$ with a residual matrix $\boldsymbol{E}$, as shown in Eq. 1.2:

$$X = PT^T + E \qquad \text{Equation 1.2}$$

where $\boldsymbol{P}$ is a matrix of the eigenvalues (scores), $\boldsymbol{T}$ is the matrix of eigenvectors (loadings), $\boldsymbol{T^T}$ is the transpose of that matrix, and **E** is the residual matrix which contains mostly noise. The scores matrix defines the relationship between each sample

in the new coordinate system, while the loadings matrix defines the relationship between the original variables (ToF-SIMS integrated ion peaks at their respective *m/z* values) and the new coordinate system (Figure 1.3).

PCA was utilized for evaluation and interpretation of amino-acid fragmentation ratios collected from ToF-SIMS spectra. More specifically, PCA was used to evaluate differences in the distributions of emitted amino acid fragment ions on the functionalized surface on which they were bound.

Chapter 2

MATERIALS AND METHODS

2.1 Chemicals

Borosilicate glass cover slips (12Cir-2) were purchased from Fisher Scientific. Toluene (certified ACS) and methylene chloride (DCM) (certified ACS) were obtained from Fisher Scientific and dried using 4-Å molecular sieves, while hydrogen peroxide (30%) (certified ACS), acetone (spectranalyzed), sulfuric acid (conc.), and ethanol (200 proof) (USP) were obtained from Fisher Scientific and used as received. 3-(Aminopropyl)trimethoxysilane (APTMS)(97%) was purchased from Alfa Aesar (Ward Hill, MA). Tetrazine-modified green fluorescent protein (referred to herein as GFP-Tet) and unmodified green fluorescent protein (referred to herein as GFP) was supplied by collaborators at Oregon State University from the Ryan Mehl research group. Strained, trans-cyclooctene, (4-nitrophenyl) 3-[(4E)-9bicyclo[6.1.0]non-4-enyl]propanoate (referred to herein as s-TCO) and strained, cis-cyclooctene, (4-nitrophenyl) 3-[(4Z)-9bicyclo[6.1.0]non-4-enyl]propanoate (referred to herein as s-CCO) was supplied by University of Delaware collaborators from the Joe Fox research group. Silicone elastomer and silicone elastomer curing agent (Sylgard 184 silicone elastomer kit) were purchased from Dow Corning Corporation (Midland, MI) (the cured product, polydimethylsiloxane, will be referred to as PDMS). Dulbecco's Phosphate Buffered Saline without calcium and magnesium (10x) was purchased from

Mediatech, Inc. All water was de-ionized, distilled over quartz and filtered by a Milli-Q water system (Millipore Co), which resulted in a resistivity of 18 MΩ cm.[27]

2.2 PDMS Stamp Synthesis

Patterned PDMS stamps were fabricated by pouring a mixture of Sylgard 184 elastomer and curing agent, utilizing a volume ratio of 10:1, into a 100-mL reusable glass beaker. The PDMS elastomer and curing agent were thoroughly mixed for a minimum of 45 seconds and then degassed inside a vacuum chamber for 2 hours. The degassed elastomer was poured into a 35-mm by 10-mm tissue culture dish (Greiner CELLSTAR) over a patterned silicon wafer master (the negative of the desired pattern) that was manufactured in the Biomedical Micro-sensor Laboratory in North Carolina State University. The elastomer and master were then cured at 70° C under 760 Torr for a period of 24 hours in a vacuum oven (VWR 1400E, Shelton Manufacturing Co., Cornelius, OR). After the elastomer was cured it was carefully removed from the master stamp by peeling, and cut to an appropriate size with a razor blade, ensuring the patterned area on the PDMS stamp was retained. This process was used with a master that produced a PDMS stamp containing alternating 80-µm-wide raised lanes and 40-µm-wide depressed lanes, approximately 1 cm in length.

2.3 Substrate Cleaning

Borosilicate glass cover slips (12Cir-2, Fisher Scientific) were pre-cleaned by sonication in a solution of 1:1 acetone/ethanol for a period of fifteen minutes and allowed to dry in ambient conditions within a fume hood. Dry glass slides were immersed in a Piranha solution (v/v 7:3 98% H_2SO_4:30% H_2O_2) to remove organic contaminants and placed on a 120-°C hotplate for 1 hour. Cleaned glass slides were

then rinsed three times with Milli-Q filtered water (18 MΩ cm), sonicated for 50 minutes (milli-Q water replaced every ten minutes), blown dry with compressed argon gas, and dried on a 120-°C hotplate for 30 minutes. Contact angle measurements (First Ten Ångstroms, Portsmouth, VA) were then taken with a RS170 camera using 3 sample slides, while the remaining slides were stored in a closed container until further processing.

2.4 Silanization

2.4.1 Solution-Phase Silanization

To produce aminosilane-terminated glass substrates by a solution-phase method, freshly cleaned glass substrates were transferred to a pure nitrogen atmosphere and immersed in a mixture of 3-(aminopropyl)trimethoxysilane (APTMS) (97%, Alfa Aesar, Ward Hill, MA) (100 µL) and dry toluene (20 mL) for a period of 3 hours. Substrates were then rinsed three times with dry toluene, removed from the nitrogen atmosphere, rinsed three more times with toluene, dried with compressed argon gas and allowed to further dry on a 70-°C hotplate for 60 minutes under ambient atmosphere.

2.4.2 Vapor-Phase Silanization

To produce aminosilane-terminated glass substrates by a vapor-phase method, freshly cleaned glass substrates were transferred to a Petri dish with one un-cleaned glass slide. 50 µL of APTMS was aliquoted onto the un-cleaned glass slide, the Petri dish was sealed, and the clean glass slides were exposed to the APTMS vapor for a period of 24 hours. Contact angle measurements were then taken using 3 sample slides

while the remaining slides were stored in a closed container in the vent hood until further processing.

2.5 Micro-contact Printing of s-TCO or s-CCO

Patterned PDMS stamps with alternating 80-µm-wide raised lanes and 40-µm-wide depressed lanes were cleaned by sonication in ethanol (200 Proof) for a period of ten minutes and placed in a plasma cleaner for 90 seconds (Harrick PDC-32G, room air bleeding). Wider raised lanes were selected to provide the ability to distinguish between regions that had been contacted by the stamp (80-µm-wide lanes) and regions that had not been contacted by the stamp (40-µm-wide lanes). Each stamp was then exposed to a solution of either s-TCO or s-CCO, dissolved in CH_2Cl_2 at a concentration of 0.050 mg/mL, and allowed to dry for 5 minutes. These “inked” PDMS stamps were then brought into contact with APTMS-modified glass slides for a period of 30 minutes (200 g of weight was added to the PDMS stamp to increase contact area and contact uniformity). The PDMS stamp was removed and the glass slide was rinsed three times with ethanol (200 proof) and allowed to dry. An example of the micro-contact printing scheme is shown in Figure 2.1.

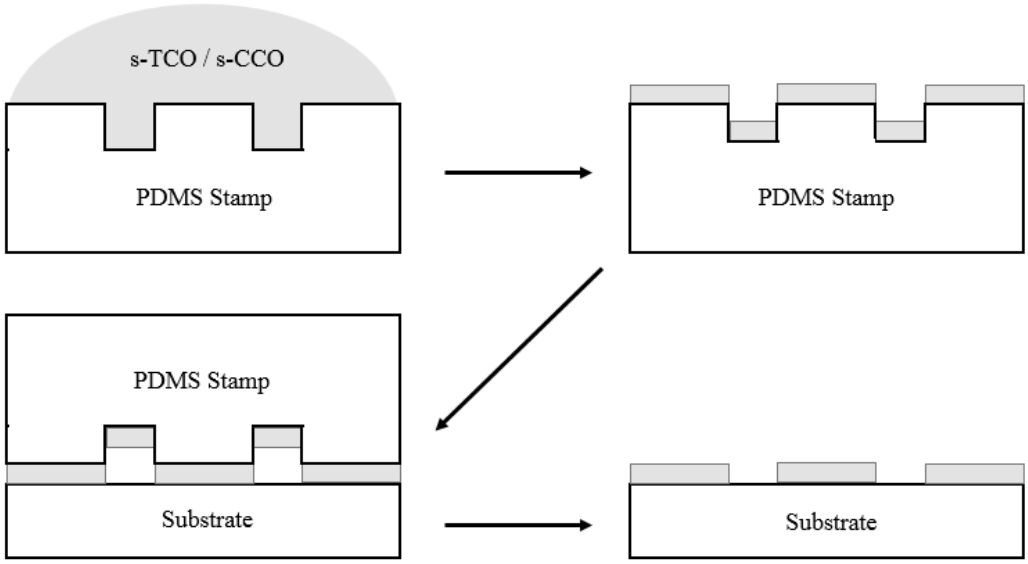

Figure 2.1 Micro-contact printing patterning scheme.

2.6 Protein Adsorption

The functionalized side of individual glass samples were completely covered with 300 µg/mL of either GFP-Tet or GFP, which was suspended in 1X-DPBS at room temperature, and incubated for a period of 30 seconds. The substrates were then rinsed three times with 1X-DPBS, rinsed for 15 minutes in 1X DPBS with 0.5% Tween 20 (solution replaced every 5 minutes), and finally rinsed in Milli-Q filtered water (18 MΩ cm) for 15 minutes (water replaced every 5 minutes). Substrates were analyzed immediately after protein adsorption. An example of the reaction scheme for the entire functionalization process is displayed in Figure 2.2.

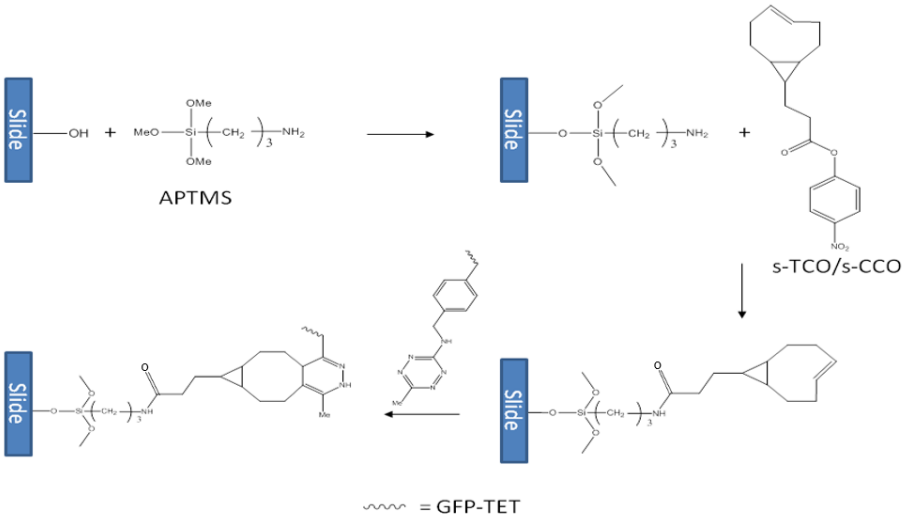

Figure 2.2 Schematic of reactions used in the functionalization and adsorption of GFP-Tet to the glass substrate. Molecular structures are not to scale.

2.7 Contact Angle Analysis

All water contact angles were obtained using a model FTA125 Contact Angle Analyzer (First Ten Ångstroms, Portsmouth, VA) with a RS170 camera and associated software. Aliquots (3 µL) of Milli-Q filtered water (18 MΩ cm) were pipetted onto glass substrates using a Distriman adjustable repeater-pipette (model u100) with Distritip (125 µL) under ambient conditions (~25% relative humidity and 25 °C). Contact angles were measured and calculated within 10 seconds of pipetting (i.e., after the water drop stopped advancing across the surface and maintained a stable shape) using the fitting program included in the FTA32 v2.0 software package.

2.8 Molecular Analysis of Patterned Surfaces by ToF-SIMS

All static TOF-SIMS spectra and images were acquired on a TOF-SIMS IV instrument (ION-TOF, GmbH; Münster, Germany), upgraded with a 25-keV Bi/Mn

liquid metal ion gun source and an incident angle of 45 degrees to the surface plane. Ion spectra were acquired using Bi_3^+ primary ions in the high-current bunched mode (high mass resolution $m/\Delta m \approx 10{,}000$ at $m/z = 29$). The typical target current of the primary ion beam was ~0.4 pA, with a pre-bunched pulse width of 30 ns and a post-bunching arrival pulse width typically less than 700 ps (calculated by the FWHM of the H^+ peak). Data collection was achieved by rastering the primary ion beam over a $500 \times 500\ \mu m^2$ area on each sample, with a typical pixel density of 128 × 128. To ensure static SIMS conditions were met the dose density was kept below 1.0×10^{12} ions/cm^2 for each sample. Because the samples were non-conductive a low-energy (~20 eV) pulsed electron beam was used for surface charge compensation. Because there were few GFP or GFP-Tet characteristic peaks in the negative-ion spectra, only the positive-ion ToF-SIMS spectra were used for compound identification. All mass spectra of the positive ion fragments were calibrated using the following spectral features and *m/z* values: H^+ (*m/z* = 1.0078503), H_2^+ (2.0157006), H_3^+ (*m/z* = 3.0235509), C^+ ((*m/z* = 12.000000), CH^+ (*m/z* = 13.0078503), CH_2^+ (*m/z* = 14.0157006), CH_3^+ (*m/z* = 15.0235509), $C_2H_3^+$ (*m/z* = 27.0235509), $C_3H_5^+$ (*m/z* = 41.0392515), $C_4H_7^+$ (*m/z* = 55.0549521), $C_5H_5^+$ (*m/z* = 65.0392515), $C_6H_5^+$ (*m/z* = 77.0392515), and $C_7H_7^+$ (*m/z* = 91.0549521). ToF-SIMS data processing was performed using SurfaceLab 6.3 (ION-TOF, GmbH; Münster, Germany) software package to obtain integrated peak areas.

2.9 Fluorescence Analysis by Fluorescence Microscope

Protein-patterned functionalized glass slides were imaged using a TE2000-s inverted fluorescence microscope (Nikon Corp., Melville, NY) with 10× (NA 0.30) Plan-Fluor objective, mercury excitation source, and CoolSNAP-Pro CCD camera

(Roper Scientific Photometrics, Trenton, NJ). Images were captured and analyzed using Image Pro Express v4.5 software package (Media Cybernetics).

2.10 Chemometrics

All principal components analysis (PCA) was performed using RStudio (RStudio Team (2015), RStudio: Integrated Development for R. RStudio, Inc., Boston, MA URL http://www.rstudio.com/.). The mass spectra of the positive-ion fragments were all calibrated using the mass fragments listed above. For each ToF-SIMS spectrum, positive-ion fragmentation peaks that could originate from the amino acids of the surface-bound protein were identified (Table 3.2), integrated, and compiled. The intensities of the relevant peaks from each spectrum were normalized to the total-ion intensity of each spectrum to correct for variation in total secondary ion yields between spectra.[7] Preprocessing of the sample matrix before PCA included mean scaling and variance scaling. Mean scaling (often referred to as "mean centering") of the data at its origin ensures that the variance in the data set is due to differences between the samples, and not differences within each sample mean.[28] Variance scaling ensures that the variance between each variable carries equal weight. For instance, if within the raw data one variable had a variance associated with it that was much larger than the rest of the variables, then that variance would dominate the first PC. The compiled data matrices were imported into RStudio for PCA processing utilizing the multivariate analysis package ChemometricsWithR (Wehrens, R., (2011). Chemometrics With R: Multivariate Data Analysis in the Natural Sciences and Life Sciences. Springer, Heidelberg.).

Chapter 3

RESULTS & DISCUSSION

3.1 Contact Angle Measurement

Contact angles were used as a yes/no verification method to determine the successful modification of the glass surface for all steps prior to micro-contact printing as reported in literature.[29–31] Six contact angle measurements were made for each reaction step (i.e., for each experiment) at ambient conditions (~25% humidity and 25°C) using the sessile-drop technique. Observed contact angles are summarized in Table 3.1, and the contact-angle measurement scheme used to calculate angles is shown in Figure 3.1. After the glass slides were cleaned in a Piranha solution to remove organic residue and expose silanol groups, a water contact-angle measurement was made. Using 3 prepared glass slide samples per experiment, a contact angle of $8.3 \pm 2.4°$ ($n = 48$) was observed for the clean glass slides. The low contact angle measured, consistent with previous unpublished work from this research group[29] ($7.6 \pm 0.6°$, $n = 30$) indicated a highly hydrophilic surface, effective removal of organic contamination, and successful creation of surface silanol groups. Sets of samples that measured contact angles greater than about 14° were re-cleaned in Piranha solution. This was rare.

Upon reaction with APTMS the surface of the glass slides significantly changed from hydrophilic to moderately hydrophobic. Surfaces produced by a solution-phase silanization method had an average contact angle of $55.2 \pm 5.7°$ ($n = 30$) while surfaces produced by a vapor-phase silanization method averaged $39.4 \pm 6.3°$ (*n*

= 18). These data are in agreement with amino-terminated layers reported in literature which have contact angle value up to 63 ± 2° for 100 percent NH_2 coverage. [32,29,33,34,35] A statistical comparison of contact angles from the Piranha-cleaned glass slides in this work compared to the APTMS-modified glass slides in this work showed that the two data sets were significantly different at the 95% confidence level ($p < 0.0001$). Together with ToF-SIMS results to be discussed later, we concluded that reactions were successful at functionalization of the surface with APTMS, producing the required amino termination required for the next reaction step.

Using a two-tailed *t*-test to compare the contact angles between the solution-phase and vapor-phase APTMS methods, a *p* value of less than 0.0001 was calculated. Not surprisingly, this *p* value indicates an extremely statistically significant difference between solution-phase and vapor-phase APTMS methods. Solution-based silanization methods have been shown to suffer from lower rates of reproducibility due to water-catalyzed solution-phase polymerization followed by precipitation of APTMS oligomers, as opposed to reaction of APTMS monomers with surface silanol groups.[36] These reports are what led us initially to try the vapor-phase methods described above. Vapor-phase methods preclude the possibility of oligomers precipitation. Overall then, based on contact-angle results here, we conclude that the resulting topography and accessibility of surface amine groups vary slightly between these methods. The topography of the vapor-phase silanization method tends to be more uniform and reproducible, but such surfaces have a lower effective surface density of exposed amine groups, whereas the solution-phase silanization method tends to be less reproducible, less uniform, and produce a higher effective surface

density of exposed amine groups. This is consistent with previously reported literature.[37,36,34]

Table 3.1 Tabulated contact-angle measurements. *Estimated 100% NH_2 coverage.[32]

	Piranha-cleaned glass[29]	APTMS- modified glass[30]	t-test two-tailed APTMS solution-phase vs vapor-phase
Literature Results	7.6 ± 0.6° *n*= 30	63 ± 2°* *n* not reported	*p* not reported
Experimental	8.3 ± 2.4° *n*= 48	55.2 ± 5.7° *n*= 30 solution-phase 39.4 ± 6.3° *n*= 18 vapor-phase	$p < 0.0001$

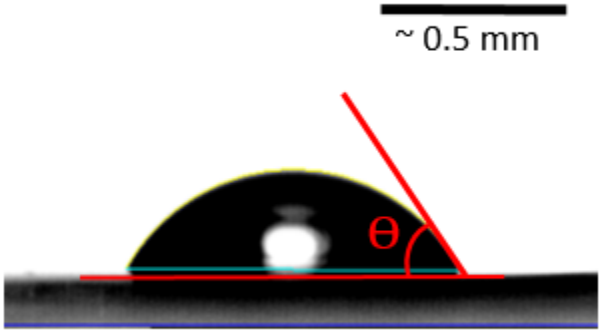

Figure 3.1 Photomicrograph of contact-angle measurement scheme. Contact angles θ were measured and calculated within 10 seconds of pipetting (i.e., after the water drop stopped advancing across the surface and maintained a stable shape) using the fitting program included in the FTA32 v2.0 software package.

3.2 ToF-SIMS Characterization Results

3.2.1 APTMS-Modified Substrate

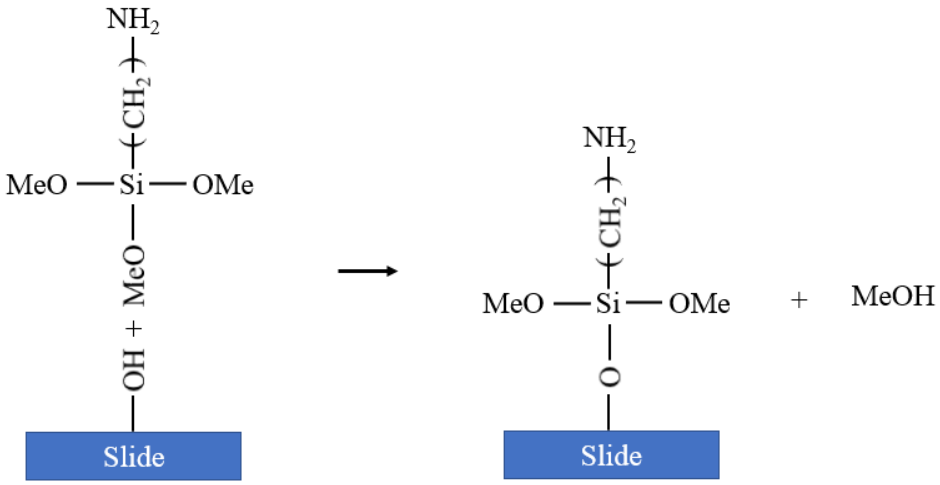

Figure 3.2 Presumed reaction scheme for surface silanol groups and APTMS.

The ToF-SIMS spectra obtained for APTMS-modified substrates were primarily dominated by secondary-ion fragment peaks indicative of pure hydrocarbons (i.e., C_xH_y), and silicon-, oxygen-, and nitrogen-containing hydrocarbons (i.e., $C_vH_wN_xO_ySi_z$). The most intense fragment peaks were observed at *m*/*z* 27.0229, 28.0184, 30.0343, 39.0228 and 41.0396, indicative of the fragments $C_2H_3^+$, CH_2N^+, CH_4N^+, $C_3H_3^+$, $C_3H_5^+$, respectively. All of these fragment ions, and others, are consistent with an APTMS-functionalized glass surface. Comparing the Si^+ peak at *m*/*z* 27.9766 of a Piranha-cleaned glass surface (Figure 3.3, high-resolution inset) with the same spectral region for an APTMS-modified surface (Figure 3.4, high-resolution

inset) indicates the presence of two new features at *m*/*z* 28.0189 (CH_2N^+) and 28.0302 ($C_2H_4^+$). Although these peaks overlap, the mass accuracy of ToF-SIMS and excellent *S/N* ratio of these spectra give us great confidence in the above assignments which differ from their theoretical values only by 6.4 and 39.2 ppm, respectively. This indicates that APTMS reacted with the surface of the Piranha-cleaned glass slide. As mentioned above, negative-mode ToF-SIMS did not provide additional insightful information and will not be discussed further.

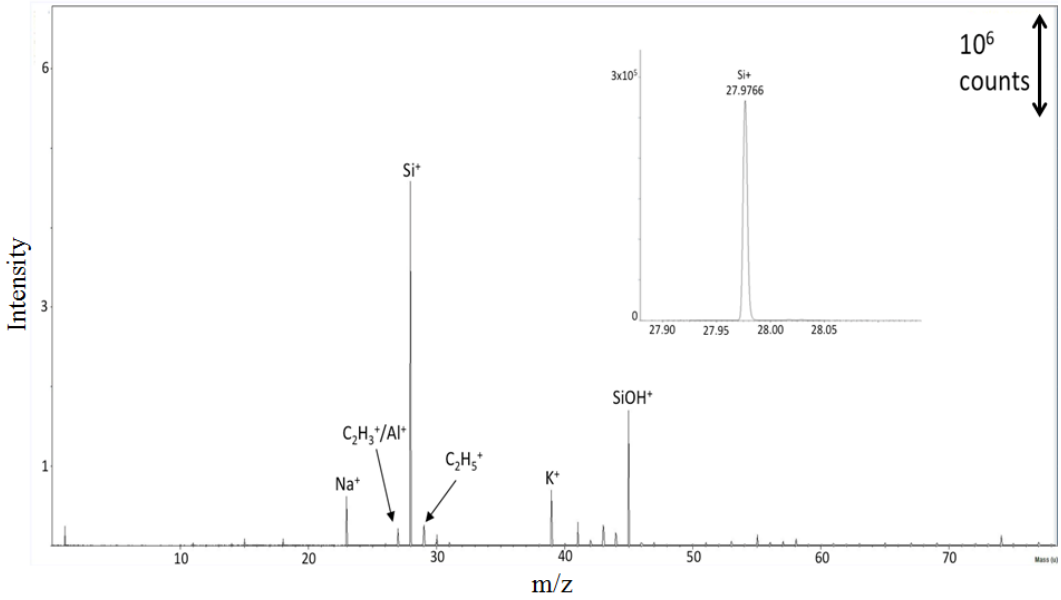

Figure 3.3 ToF-SIMS positive-ion spectrum of a clean borosilicate glass cover slip with a high-resolution inset spectrum of the Si^+ fragment region. Note that the inset spectrum shows no organic species, unlike the high-resolution inset in Figure 3.4.

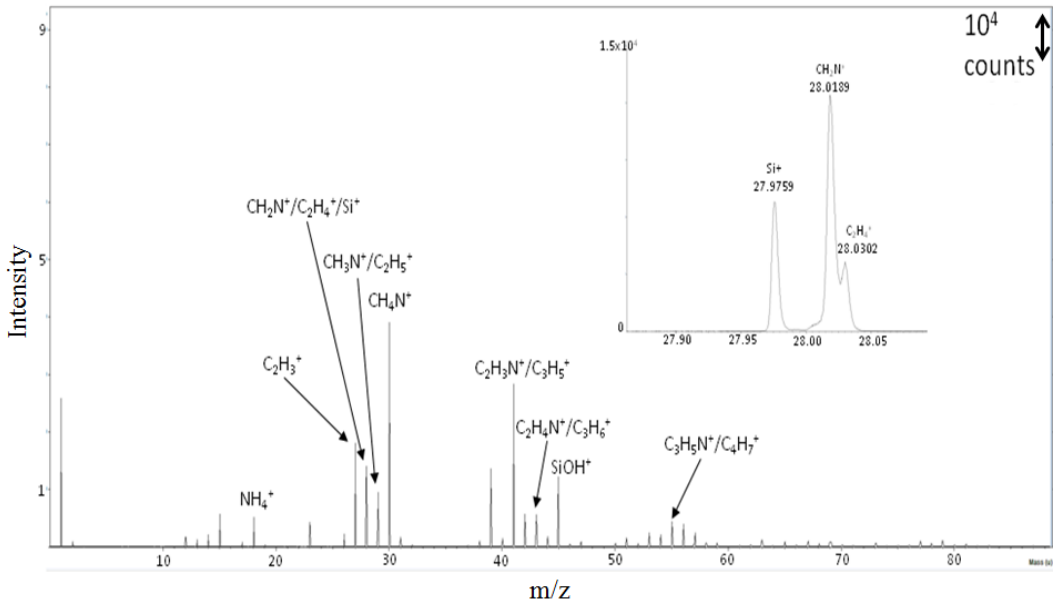

Figure 3.4 ToF-SIMS positive-ion spectrum of an APTMS-modified borosilicate glass cover slip with a high-resolution inset spectrum of the Si^+ fragment region. Note that the inset spectrum shows the presence of organic species, unlike the high-resolution inset in Figure 3.3.

3.2.2 s-TCO-Modified or s-CCO-Modified Substrates

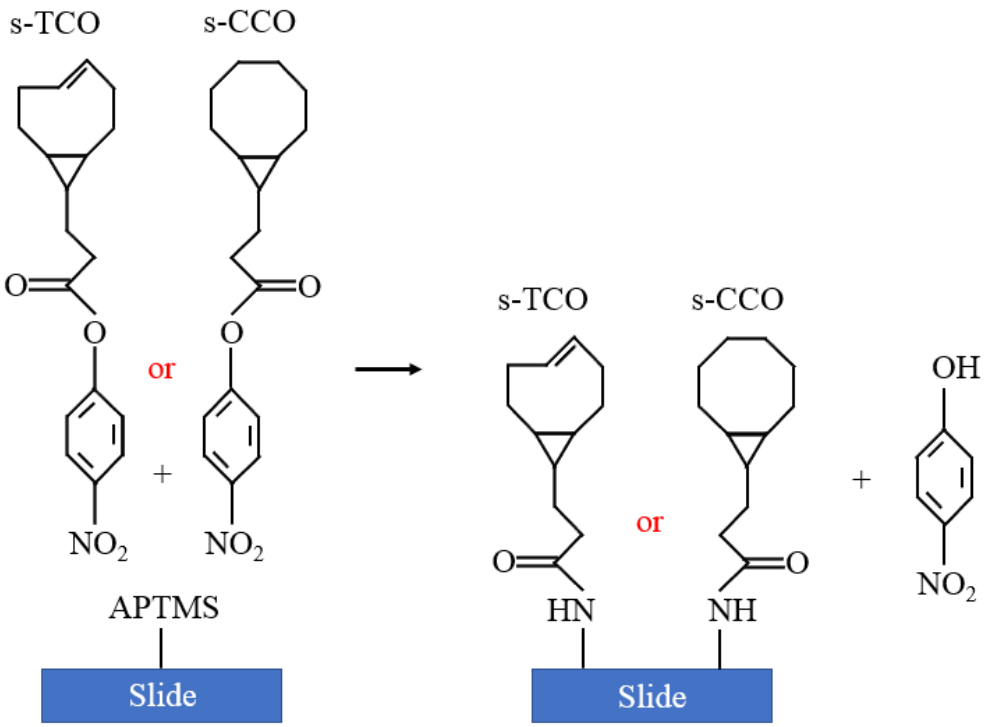

Figure 3.5 Strained, trans-cyclooctene (s-TCO) or strained, cis-cyclooctene (s-CCO) surface-modification scheme.

The ToF-SIMS spectra obtained for the s-TCO- or s-CCO-modified substrates were similar to the APTMS-modified substrate in some ways upon cursory inspection: they were also dominated by peaks indicative of pure ($C_xH_y^+$), oxygen-containing ($C_xH_yO_z^+$), and nitrogen-containing ($C_xH_yN_z^+$) hydrocarbon fragments. The most intense fragment peaks (and their assignments) were observed at *m*/*z* 29.0391 ($C_2H_5^+$), 41.0399 ($C_3H_5^+$), 55.0205 ($C_3H_3O^+$), 55.0555 ($C_4H_7^+$), 67.0567 ($C_5H_7^+$), and 79.0555 ($C_6H_7^+$). All of these fragments are consistent with secondary ions from s-TCO or s-

CCO, and the mass errors of the assignments ranged from only 0 to 38 ppm, making assignment confidence extremely high. Represented in the inset spectra of Figure 3.6 are the high-resolution spectra of the nominal 57 and 81 *m/z* regions. Fragments of $C_3H_5O^+$, $C_4H_9^+$, and $C_6H_9^+$, not seen in ToF-SIMS spectra prior to reaction with s-TCO or s-CCO, were also observed and are characteristic fragment peaks of s-TCO and s-CCO.

Also notable from the ToF-SIMS spectra was that as s-TCO or s-CCO was patterned over APTMS, many of the characteristic ion peaks for APTMS decreased in intensity, while characteristic ion peaks for s-TCO or s-CCO increased. The decrease in APTMS-related ion peaks is due to the APTMS being covered by a monolayer of the s-TCO or s-CCO on the substrate, while the increase in s-TCO- and s-CCO-related peaks is due to the addition of those on the surface by reaction with APTMS.

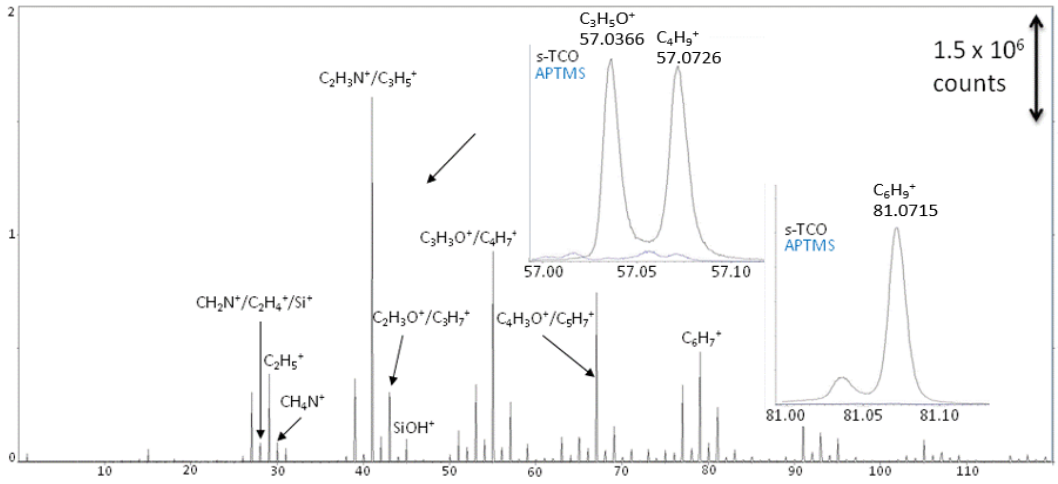

Figure 3.6 ToF-SIMS positive-ion spectrum of s-TCO-modified or s-CCO-modified glass cover slip (both molecules gave the same ToF-SIMS spectra and are generally indistinguishable). The high-resolution inset spectra show some characteristic mass fragments of s-TCO or s-CCO (black), while APTMS (blue) is barely visible above the baseline at this vertical scale.

3.2.3 GFP-Modified or GFP-Tet-Modified Substrate

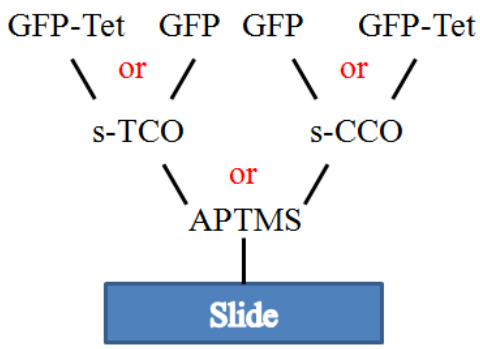

Figure 3.7 GFP or GFP-Tet modification scheme. Following functionalization of surface hydroxyl groups with amine-terminated APTMS and functionalization of those surfaces by s-TCO or s-CCO, samples were reacted with GFP or GFP-Tet. The above combined scheme shows all four possible final surfaces.

It is known from the TOF-SIMS literature for surfaces modified by proteins that TOF-SIMS does not generally produce spectra of high-mass molecular-ion peaks, as for example does matrix-assisted laser desorption ionization (MALDI).[26] Molecular-ion peaks were not expected here for either GFP- or GFP-Tet-modified surfaces.

Instead, a great deal of useful information about surfaces modified by proteins has been extracted by TOF-SIMS data from such surfaces using known fragment peaks of individual amino acids comprising those proteins. A comprehensive list of all known peaks associated with the amino acids that comprise proteins was compiled from literature and used here for identification, as shown in Table 3.2.[38,39,40,41,42]

Following reaction with the protein GFP or the GFP-Tetrazine adduct, the most intense mass fragments (and their assignments) were observed at *m/z* 28.0189 (CH_2N^+), 30.0401 (CH_4N^+), 41.0272 ($C_2H_3N^+$), 55.0197 ($C_3H_3O^+$), and 70.0664 ($C_4H_8N^+$), as seen in Figure 3.8 All of these species were consistent with mass fragments identifiable in the constructed list of characteristic amino acid ion fragments. One notable problem was that many of the observed amino acid ions were also consistent with observed ions of both APTMS and s-TCO or s-CCO. This made identification of specific secondary ion fragments due to protein alone (i.e., unique protein marker peaks), more challenging.

Represented in Figure 3.8 is a high-resolution inset spectrum of the nominal 43 *m/z* region, which shows the appearance of the ion at *m/z* 43.0421. This fragment can be attributed to APTMS as well as to the amino acid lysine. However, because the $C_2H_5N^+$ ion signal was suppressed when s-TCO or s-CCO was patterned over the APTMS layer, the reappearance of the fragment signal upon reaction with protein indicates that the signal in this situation is highly likely due to the amino acid in the protein, and not the APTMS as its source. The pattern of ions being suppressed after application of s-TCO or s-CCO and then reemerging after application of the protein layer was also observed for other amino acid mass fragments.

Also represented in the high-resolution inset spectrum in Figure 3.8 is the appearance of a peak at *m/z* 43.0293 ($CH_2N_2^+$). This protein fragment peak is indicative of arginine, and was only observed after the substrate had been incubated with GFP or GFP-Tet, but not with prior reaction steps. Mass accuracy for this peak was excellent, with the observed position differing by only 7.3 ppm from the theoretical position of *m/z* 43.0297, providing extremely high confidence in this

assignment. $C_xH_yN_z^+$ peaks with *x* greater than 3 were not seen in any surface layers prior to the application of GFP or GFP-Tet, and were therefore identified as originating from amino acids in GFP, in accordance with the compiled protein peak list of Table 3.2.

In the case of oxygen-containing mass fragments that were found to be associated with s-TCO or s-CCO and GFP-Tet or GFP, these fragment ions were not used for protein identification. Only the unique characteristic amino acid fragments (i.e., not also observed in prior substrate reaction steps) were utilized for identification of the protein layer (GFP) or protein-tetrazine (GFP-Tet) layer.

Table 3.2 List of characteristic amino acids and their secondary ion fragments used for ToF-SIMS analysis.[20,38,39,40,41,42]

Amino Acid	Abbrev.	Fragment	m/z
Alanine	Ala, A	$C_2H_6N^+$	44.0500
		$C_2H_3N^+$	41.0265
		CH_2N^+	28.0187
Arginine	Arg, R	$CH_3N_2^+$	43.0297
		$C_2H_7N_3^+$	73.0640
		$C_4H_{10}N_3^+$	100.0876
		$C_5H_8N_3^+$	110.0718
		$C_4H_8N^+$	70.0657
		$CH_5N_3^+$	59.0484
		$C_4H_{11}N_3^+$	101.0953
		$C_5H_{11}N_4^+$	127.0932
Asparagine	Asn, N	$C_3H_4NO^+$	70.0293
		$C_3H_7N_2O^+$	87.0559
		$C_3H_6NO_2^+$	88.0399
		$C_4H_4NO_2^+$	98.0242
Aspartic Acid	Asp, D	$C_3H_6NO_2^+$	88.0399
Cysteine	Cys, C	$C_2H_6NS^+$	76.0221
		CHS^+	44.9800
		$C_2H_3S^+$	59.0000
Glutamine	Gln, Q	$C_4H_6NO^+$	84.0449
Glutamic Acid	Glu, E	$C_4H_6NO^+$	84.0449
		$C_4H_8NO_2^+$	102.0579
		C3H4O+	56.0000
		$C_3H_7O^+$	83.0500
Glycine	Gly, G	CH_4N^+	30.0343
Histidine	His, H	$C_4H_5N_2^+$	81.0453
		$C_4H_6N_2^+$	82.0532
		$C_5H_8N_3^+$	110.0718
Hydroxyproline	Hyp	$C_4H_8NO^+$	86.0606
Isoleucine	Ile, I	$C_5H_{12}N^+$	86.0970
Leucine	Leu, L	$C_5H_{12}N^+$	86.0970
		$C_5H_{10}N^+$	84.0900
Lysine	Lys, K	$C_5H_{10}N^+$	84.0813
		$C_2H_5N^+$	43.0420
		$C_3H_6N^+$	56.0500
		$C_4H_6NO^+$	84.0449
Methionine	Met, M	$C_2H_5S^+$	61.0094
		$C_4H_8NO_2^+$	102.0600

Table 3.2 (continued)

Phenylalanine	Phe, F	$C_8H_{10}N^+$	120.0813
		$C_9H_7O^+$	131.0575
		$C_9H_8O^+$	132.0575
Proline	Pro, P	$C_4H_6N^+$	68.0501
		$C_4H_8N^+$	70.0657
Serine	Ser, S	$C_2H_6NO^+$	60.0449
		$C_3H_3O_2^+$	71.0133
Threonine	Thr, T	$C_4H_5O^+$	69.0340
		$C_3H_8NO^+$	74.0606
Tryptophan	Trp, W	$C_9H_8N^+$	130.0657
		$C_{11}H_8NO^+$	170.0606
		$C_{10}H_{11}N^+$	159.1000
Tyrosine	Tyr, Y	$C_7H_7O^+$	107.0497
		$C_8H_{10}NO^+$	136.0777
Valine	Val, V	$C_4H_{10}N^+$	72.0813
		$C_5H_7O^+$	83.0497

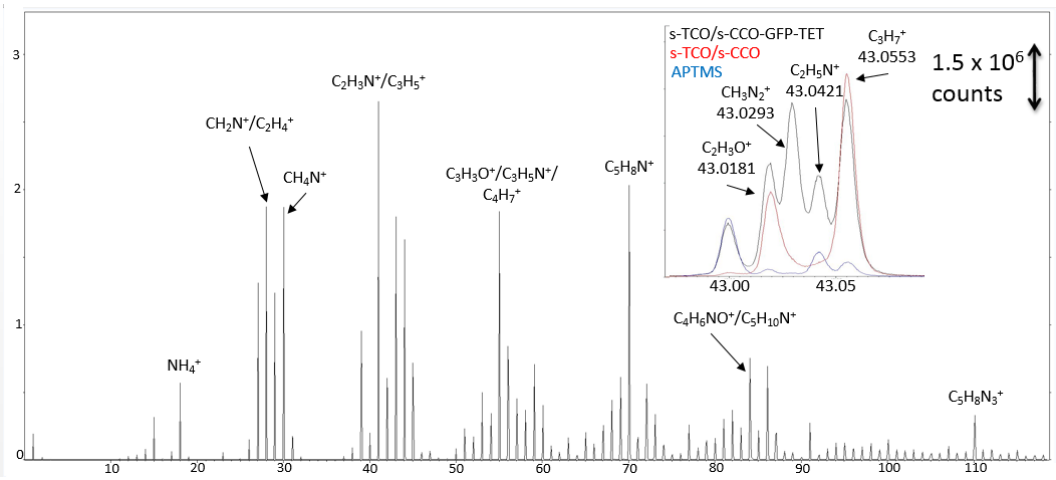

Figure 3.8 ToF-SIMS positive-ion spectra of an s-TCO- or s-CCO-modified glass cover slip that has been incubated with GFP-Tet. The high-resolution inset spectrum is displayed to show the appearance of the $CH_3N_2^+$ peak which is a characteristic secondary ion associated with several amino acids, but not with prior reaction steps.

3.2.4 ToF-SIMS Image Analysis

As described in the introduction, analysis of ToF-SIMS data can be done for data in spectrum or image formats. Because surfaces were patterned here using micro-contact printing, and since the length scale of the patterned features was a few tens of micrometers, the collection of ToF-SIMS data in image format offered an excellent opportunity to obtain molecular information on an appropriate lateral length scale. This is certainly one of the great strengths of ToF-SIMS.

One way to think about ToF-SIMS data in image format is to imagine that the analysis area in the *x, y* plane of the sample surface is divided into many small square regions. The work herein used 128 by 128 such regions, totaling 16,384 regions. In each region or pixel, all data for an entire high-resolution mass spectrum is contained. It is the analysis of such data that we discuss below.

Finally, we selected a PDMS stamp pattern that provided an unambiguous means of identifying and distinguishing reacted patterned regions and unreacted patterned regions. Wider raised lanes (i.e., those that make contact with the surface during the printing step) were selected to provide the ability to distinguish between regions that had been contacted by the stamp (80-μm-wide lanes) and regions that had not been contacted by the stamp (40-μm-wide lanes), as seen in Figure 2.1.

When examining a ToF-SIMS spectrum of an APTMS modified glass surface, the predominant ion in the spectrum was $SiOH^+$. By assigning each pixel a color based on this ion's intensity in that pixel, a false-color image can be used to represent the presence and local coverage of APTMS, as shown in the representative image of Figure 3.9(A). Because of the surface-sensitivity of ToF-SIMS, the image of this mass fragment (or any other mass fragment) is associated with the top 1-2 monolayers of the surface. Upon micro-contact printing of s-TCO (fascile reaction with terminal

amine groups of APTMS is expected) or s-CCO (fascile reaction with terminal amine groups of APTMS is not expected), a clear emergence of the $C_6H_9^+$ ion signal, assigned to a green false-color scale, was observed in representative images (e.g., Figure 3.9(B)). In the wide lanes (s-TCO- or s-CCO-patterned), this image shows a high green intensity ($C_6H_9^+$, a marker for s-TCO and s-CCO) and a low red intensity ($SiOH^+$, a marker for APTMS). In the narrow lanes (not s-TCO- or s-CCO-patterned), the image also shows a low green intensity and a high red intensity in the unpatterned lanes (i.e., regions of the substrate that did not contact the inked stamp). From these results, we conclude that s-TCO and s-CCO reacted with APTMS only in regions contacted by the stamp, as expected.

The $C_5H_{12}N^+$ ion (observed *m/z*: 86.1016; theoretical *m/z*: 86.0970; mass error 54 ppm), a known fragment of leucine, was used for protein identification in ToF-SIMS images, and assigned a blue false-color scale. Figure 3.9 (C) is a representative ToF-SIMS image of a sample that had been functionalized with APTMS, micro-contact printed with an uninked (i.e., no s-TCO or s-CCO applied), and then incubated with GFP or GFP-Tet. Such a sample served as a control for any effect that contamination transferred from the stamping process might have had on the sample's reactivity with protein (GFP) or protein-tetrazine (GFP-Tet). This image shows no spatial contrast in the various false-color schemes, indicating that very little, if any, such contamination-driven protein adsorption or reactivity occurred.

Figures 3.9 (D) and (E) display representative ToF-SIMS images of samples that had been functionalized with APTMS, then micro-contact printed with s-CCO (Figure 3.9 (D)) or s-TCO (Figure 3.9 (E)). Both sample types were then incubated with GFP-Tet. Fascile reaction of s-CCO with GFP-Tet is not expected in s-CCO

lanes. Fascile reaction of s-TCO with GFP-Tet is expected in s-TCO lanes. The high red intensity in the 40-µm-wide (the narrower lanes) of these images indicates that GFP-Tet did not adsorb on or react with the APTMS regions, as expected. This result is the control experiment for non-specific protein adsorption on APTMS.

Continuing our discussion of the ToF-SIMS images in Figures 3.9 (D) and (E), the virtual replacement of green intensity ($C_6H_9^+$, a marker for s-CCO and s-TCO) by blue intensity ($C_5H_{12}N^+$, a marker for GFP-Tet) in the 80-µm-wide wide lanes indicates that protein adsorption and/or reaction occurred on the s-CCO and s-TCO lanes. The ideal but unrealistic experimental result would have been one in which Figure 3.9 (D) consisted of narrow red lanes (indicating APTMS only with no protein reaction in these narrow lanes), and wide green lanes (indicating no protein adsorption nor reaction with s-CCO), since reaction of the protein-tetrazine adduct with the cis-cyclooctene moiety is not expected. Likewise, the ideal but unrealistic experimental result for Figure 3.9 (E) would consist of narrow red lanes (indicating APTMS only, with no protein reaction in these narrow lanes), and wide blue lanes (indicating fascile reaction of the GFP-Tet with s-TCO).

The above results, while ideal, are not realistic because they do not take into account the competing effects of non-specific adsorption of GFP-Tet with s-CCO regions and the reaction of GFP-Tet with s-TCO regions. While it might have been possible to tease out these different phenomena based on their different kinetic time scales, such incubation experiments were not performed. The fact that the resulting ToF-SIMS images in Figures 3.9 (D) and (E) were very similar under the conditions used here indicates either one of two likely outcomes: 1.) non-specific physical adsorption of protein (GFP-Tet) on the s-CCO regions resulted in a surface very

similar to reactive chemical adsorption of protein (GFP-Tet) on the s-TCO regions; or 2.) any chemical adsorption of protein caused by the reaction of GFP-Tet with s-TCO, the desired reaction pathway, was overwhelmed by the concurrent or subsequent physical adsorption of protein, regardless of whether that adsorption occurred on s-CCO or s-TCO. Additional light is shed on these alternatives in experiments described below.

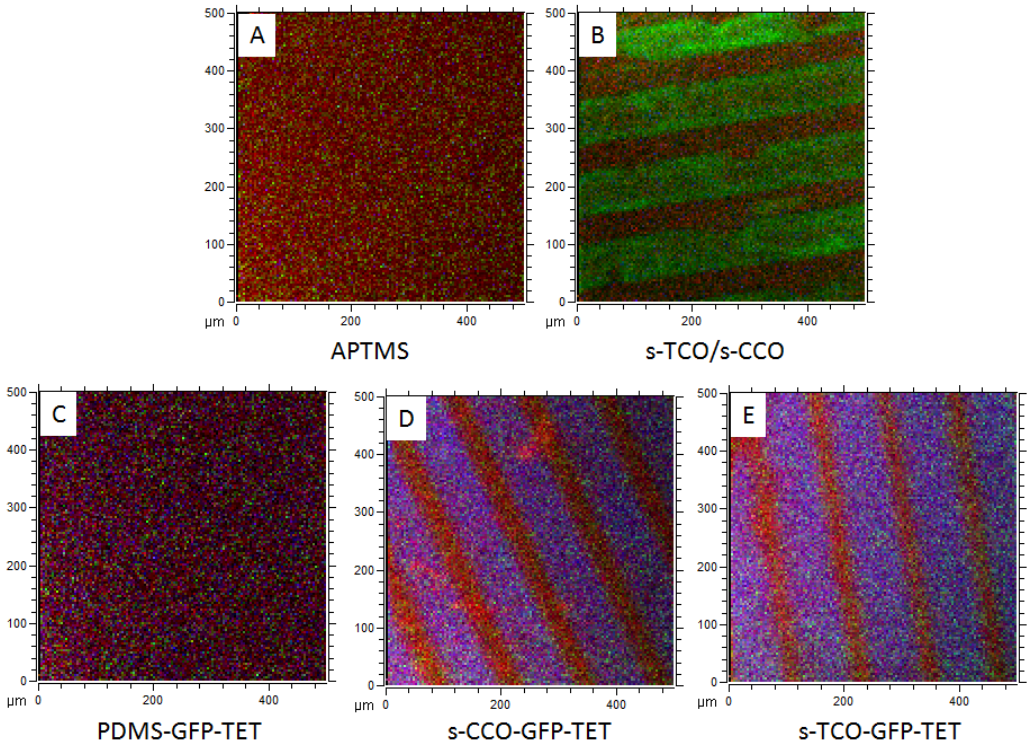

Figure 3.9 ToF-SIMS positive-ion images, 500 µm by 500 µm, of reaction steps associated with the functionalization of glass slides using single, characteristic fragment ion peaks for image contrast. The narrow lanes (40-µm-wide) are regions that were not contacted with the PDMS stamp, whether inked or not. The wide lanes (80-µm-wide) are regions that were contacted with the PDMS stamp, whether inked or not. A red false-color scale is used above to represent $SiOH^+$ intensity, a good marker for both clean glass, and, in this case, APTMS. A green false-color scale is used above to represent $C_6H_9^+$ intensity, a good marker for both s-CCO and s-TCO. A blue false-color scale is used above to represent $C_5H_{12}N^+$ intensity, a good marker for leucine in protein. (A) APTMS-modified substrate. (B) s-TCO-modified or s-CCO-modified substrate (images of both species were indistinguishable). (C) Substrate stamped with clean (i.e., uninked) PDMS stamp, followed by incubation in GFP or GFP-Tet (images of both species were indistinguishable). (D) Micro-patterned s-CCO-modified substrate (wide lanes) incubated with GFP-Tet. (E) Micro-patterned s-TCO-modified substrate (wide lanes) incubated with GFP-Tet.

3.3 Fluorescence Imaging of Protein Patterns

Protein patterns of GFP and GFP-Tet were imaged by fluorescence microscopy and a sample set of images is shown in Figures 3.10 (A) – (D). The micro-contact patterning process produced visible spatial contrast in fluorescence images of alternating 40-μm-wide lanes of amine-terminated groups from APTMS and 80-μm-wide lanes with one of four conditions, as described in the caption of Figure 3.10, to be discussed shortly. In order to quantify the image contrast between the different resulting patterned surface chemistries, an analysis of the fluorescence intensity in all image pixels was carried out. Figure 3.11 is a schematic diagram of the method used for the following analysis, shown with an example fluorescence image. The images were first background corrected for autofluorescence in the glass slides by a pixel-wise subtraction of the average pixel intensity from a clean, unfunctionalized glass slide with all other experimental parameters held constant. Images were then converted to 24-bit contrast using ImagePro Express v4.5 (Media Cybernetics). For each sample, 8 areas of interest were selected to comprise alternating regions of the patterned surfaces consisting of equal areas of the same lanes (case A: GFP-only lanes separated by amine-terminated lanes; case B: GFP-Tet lanes separated by amine-terminated lanes). Pixel intensity histograms were then plotted using ImageJ v1.48 (Schneider, C.A., Rasband, W.S., Eliceiri, K.W. "*NIH Image to ImageJ: 25 years of image analysis*". Nature Methods 9, 671-675, 2012.), giving $I_{protein}$ (in GFP-only or GFP-Tet lanes) and $I_{background}$ (in amine-terminated lanes). These values were obtained by locating the centroid of the pixel intensity histogram derived from pixels in the relevant lanes. Histogram intensities in the narrow lanes were easily distinguished from those in the wide lanes. Each group of pixel intensities was calculated and is shown in Table 3.3. For example, the s-TCO-GFP and s-CCO-GFP slides were

prepared from the same group of glass slides that were prepared on the same day with APTMS. This helped ensure consistency and uniformity of APTMS within the set of slides used for each experimental condition. Table 3.4 shows the calculated relative protein contrast defined by the ratio ($I_{protein}/I_{background}$) for all experimental groups combined.[43]

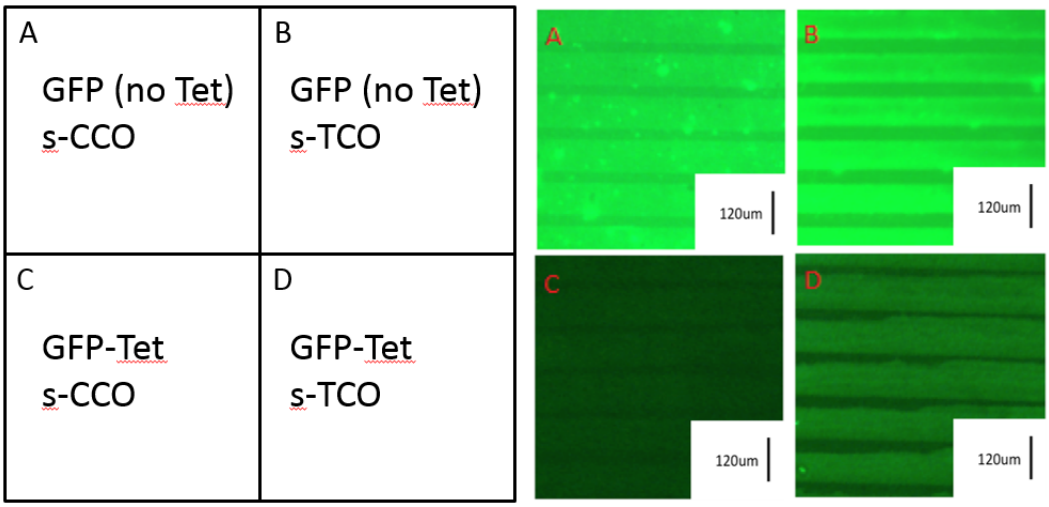

Figure 3.10 Representative fluorescence microscopy images of micro-contact patterned samples. Image contrast is derived from the presence of green fluorescent protein, GFP. The narrow lanes (40-µm-wide) are regions that were not contacted with the PDMS stamp, while the wide lanes (80-µm-wide) are regions that were contacted with the PDMS stamp. (A) micro-contact printed s-CCO in the wide lanes, followed by incubation in GFP (no GFP-Tet). This served as a control for non-specific adsorption in the absence of both the tetrazine adduct required for reaction with cyclooctene, and the unreactive cis- isomer, s-CCO. (B) micro-contact printed s-TCO in the wide lanes, followed by incubation in GFP (no GFP-Tet). This served as a control for non-specific adsorption in the absence of the tetrazine adduct required for reaction with cyclooctene, but in the presence of the reactive trans- isomer, s-TCO. (C) micro-contact printed s-CCO in the wide lanes, followed by incubation in GFP-Tet. This served as a control for non-specific adsorption in the presence of the tetrazine adduct required for reaction with cyclooctene, but with the unreactive cis- isomer, s-CCO. (D) micro-contact printed s-TCO in the wide lanes, followed by incubation in GFP-Tet. This served as the sample condition in which both the tetrazine adduct required for reaction with cyclooctene, and the reactive trans- isomer, s-TCO was present in the wide lanes.

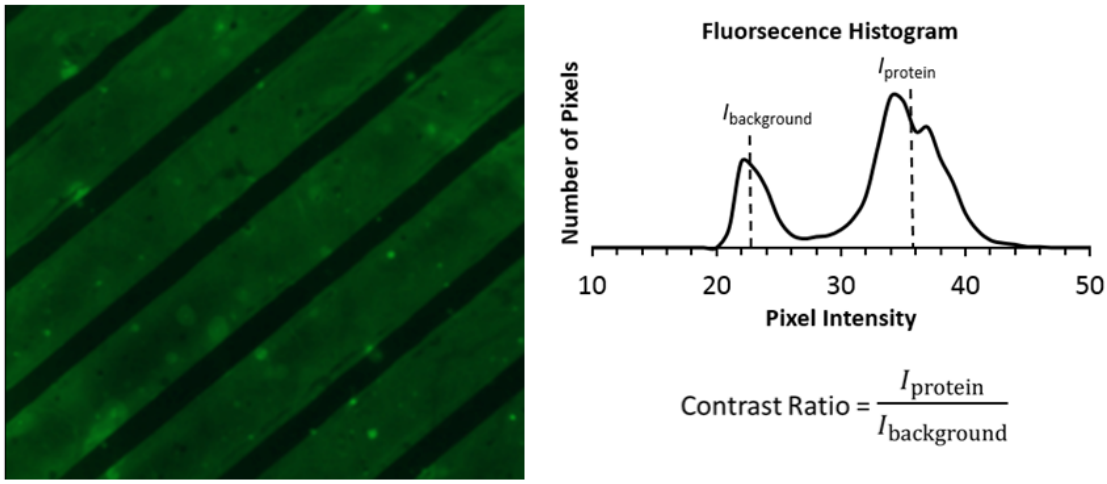

Figure 3.11 Representative schematic diagram of the method used to calculate pixel intensity of fluorescent intensity.

3.3.1 GFP-Modified Substrate

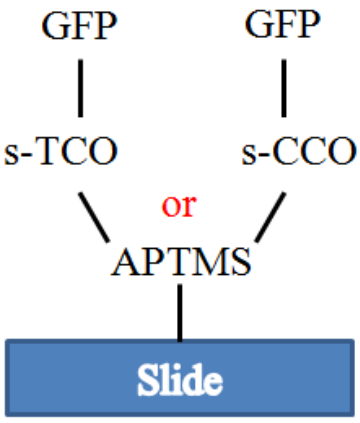

Figure 3.12 GFP modification scheme.

Unmodified GFP (i.e., no tetrazine adduct) was used as a control for fluorescence studies, selected so that the interactions between this protein and the surface were associated with non-specific binding only. The experiment is depicted in Figure 3.11. Without the tetrazine adduct, the GFP protein cannot react with the surface, regardless of whether the wide lanes contain s-CCO or s-TCO. The intensity ratios for the first pair of results in Table 3.3 were both around 3.2 to 3.3, with no significance in the difference (p = 0.0517). In the absence of reactivity, non-specific adsorption results in about the same amount of protein adsorption, as expected.

For specific, reactive bonding, bioorthogonal conditions are defined as the inverse electron-demand ligation between tetrazine and trans-cyclooctene.[15,16,44–46] The experiment is depicted in Figure 3.12. The second and third pair of results in

Table 3.3 show the relative contrast in fluorescence ($I_{protein}/I_{background}$) for both s-TCO- and s-CCO-functionalized wide lanes ($I_{protein}$) vs. amine-terminated narrow lanes ($I_{background}$). The first pair of results was obtained by the solution-phase APTMS method, while the second pair of results was obtained by the vapor-phase APTMS method. A two-tailed *t*-test of fluorescence intensity ratios between functionalized and amine-terminated lanes was calculated to be statistically different ($p < 0.0001$, two-tailed) for both solution-phase and vapor-phase APTMS, indicating that the fluorescence associated with non-specific adsorption was greater in the functionalized lanes than in the amine-terminated lanes. A slightly better protein contrast was observed for the solution-phase APTMS than for the vapor-phase APTMS.

3.3.2 GFP-Tet-Modified Substrate

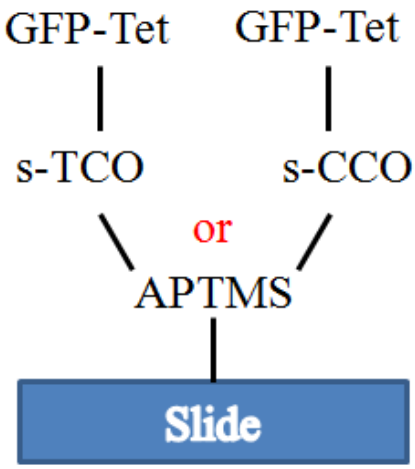

Figure 3.13 GFP-Tet modification scheme

The location of bound tetrazine in relation to the fluorophore of GFP causes the GFP-Tet adduct's fluorescence to be quenched approximately 11-fold compared to GFP without the tetrazine.[16] When the tetrazine reacts with s-TCO via inverse electron-demand ligation, there is removal of conjugation in the π-electron system that causes the fluorescence quenching, thereby leading to greater fluorescence intensity after reaction.[16] This effect operates in the same direction as that of increased protein adsorption due to reaction.

As seen in Table 3.4, comparison of the pixel intensities in lanes of s-TCO reacted with GFP-Tet vs. that in lanes of s-CCO showed that when utilizing the solution-phase APTMS method, there was, on average, $(42.9 \pm 0.9)/(4.9 \pm 0.5) = 8.8 \pm$

0.1 times more pixel intensity in the s-TCO lanes. The vapor-phase method produced pixel intensities that were, on average, $(29.0 \pm 0.7)/(8.5 \pm 0.6) = 3.41 \pm 0.07$ times greater in the s-TCO lanes than in the s-CCO lanes. These results were consistent with expectations that the GFP-Tet reacts with s-TCO and not s-CCO, resulting both in less fluorescence quenching for the former, and a greater local protein concentration for the former, due to reaction.

The GFP-Tet that adsorbed in the s-CCO-patterned lanes did so though non-specific adsorption, and the fluorescence remained quenched due to the π-electron system of tetrazine in the unreacted GFP-Tet. As was discussed previously, the method in which APTMS is applied to the surface affects the surface density of accessible amine groups, which in turn affects the surface density of s-TCO or s-CCO reactive sites in the patterned lanes. The differences between fluorescence intensities between these two functionalization methods for APTMS (i.e., solution- vs. vapor-phase) suggests that there was a higher surface density of s-TCO molecules for GFP-Tet to react with when the solution-phase APTMS method was used.

Table 3.3 Protein contrast comparison and summary. Each set of samples in the Experimental Conditions row are tabulated from a set of samples that were silanated together on a specific day (ex. s-TCO-GFP and s-CCO-GFP were reacted with glass slides that were silanated and functionalized on the same day and within the same experiment as APTMS conditions vary from experiment to experiment)

Experimental Conditions		Binding Lane Pixel Intensity	Amine Lane Pixel Intensity	$I_{protein}/I_{background}$	*t*-test, two-tailed s-TCO vs. s-CCO Intensity ratio
Surface Chemistry	Experiment Design				
s-TCO-GFP (solution-phase APTMS method)	Control for cis- vs. trans- CCO w/o Tet	42.5 ± 1.6 *n*= 12	12.7 ± 0.8 *n*= 12	3.32 ± 0.08	p = 0.0517
s-CCO-GFP (solution-phase APTMS method)		30.5 ± 1.1 *n*= 14	9.6 ± 0.6 *n*= 14	3.19 ± 0.07	
s-TCO-GFP-Tet (solution-phase APTMS method)	Control for cis- vs. trans- CCO with Tet (solution-phase)	42.9 ± 0.9 *n*= 15	14.1 ± 0.6 *n*= 15	3.04 ± 0.05	p < 0.0001
s-CCO-GFP-Tet (solution-phase APTMS method)		4.9 ± 0.5 *n*= 16	3.3 ± 0.5 *n*= 16	1.5 ± 0.2	
s-TCO-GFP-Tet (vapor-phase APTMS method)	Control for cis- vs. trans CCO with Tet (vapor-phase)	29.0 ± 0.7 *n*= 14	13.3 ± 0.6 *n*= 14	2.18 ± 0.05	p < 0.0001
s-CCO-GFP-Tet (vapor-phase APTMS method)		8.5 ± 0.6 *n*= 14	5.4 ± 0.5 *n*= 14	1.6 ± 0.1	
Uninked (clean) PDMS stamped glass slide (solution-phase APTMS method)	Control: APTMS only	No lane pattern; 1.6 ± 0.6 *n*= 4	No lane pattern; 1.6 ± 0.6 *n*= 4	1.0 ± 0.6	Not applicable

Table 3.4 Ratio of s-TCO/s-CCO pixel intensities.

Surface Chemistry	Experiment Design	Pixel Intensity Ratio	*n*
s-TCO-GFP or s-CCO-GFP	Control for cis- vs. trans- CCO w/o Tet	1.39 ± 0.05	8
s-TCO-GFP-Tet or s-CCO-GFP-Tet	Control for cis- vs. trans- CCO with Tet (solution-phase)	8.8 ± 0.1	27
s-TCO-GFP-Tet or s-CCO-GFP-Tet	Control for cis- vs. trans- CCO with Tet (vapor-phase)	3.41 ± 0.07	28

3.4 Chemometrics

Up until this point, all analysis has consisted of univariate analysis of ToF-SIMS and fluorescence images and ToF-SIMS spectra. By careful selection of unique marker peaks for APTMS, cyclooctene, and protein we have shown that differences exist in s-CCO lanes compared to s-TCO lanes. However, interpretation of those observed differences has been somewhat limited to arguments concerning differences in non-specific protein uptake by lanes printed with the reactive vs. unreactive forms of strained cyclooctene (i.e., s-CCO vs. s-TCO). Next we focus on the multivariate method Principal Components Analysis, PCA, introduced earlier.

3.4.1 Data Preprocessing

PCA was utilized to evaluate variations in the relative intensities of amino acid fragmentation patterns collected from ToF-SIMS spectra. The differences in relative intensities can in principle provide information regarding the orientation of the surface-bound protein, a long-standing goal of the surface analysis community. For each sample spectrum, 28 characteristic amino acid peaks that originate from the

surface-bound protein was compiled (Table 3.5). This peak is a subset of the more comprehensive list in Table 3.2. As is customary in the field, the intensities of each amino acid fragment were first normalized to the total ion intensity of its spectrum in order to correct for variation in total secondary-ion yields between spectra.[7] Preprocessing of the sample matrix before PC analysis included mean scaling and variance scaling. Mean scaling (often called mean centering) of the intensity data at the origin ensures that the variance in each data set is due to differences in the sample variances and not differences in each sample mean.[28] Variance scaling (i.e., for all samples, dividing each mass fragment raw intensity mean value by the mass fragment's standard deviation) ensures that the variance between each variable carries equal weight. For instance, if within the raw data one variable had a significantly larger variance than the rest, then that variance would dominate the first principal component (PC1).

Table 3.5 Characteristic positive-ion ToF-SIMS peaks selected for principal component analysis.

Amino Acid	Mass Fragment Index	Fragment	m/z
Cysteine (C)	1	$C_2H_3S^+$	59.0000
Serine (S)	2	$C_2H_4NO^+$	58.0293
Methionine (M)	3	$C_2H_5S^+$	61.0094
Serine (S)	4	$C_2H_6NO^+$	60.0449
Asparagine (N)	5	$C_3H_4NO^+$	70.0293
Asparagine (N) Aspartic Acid (D)	6	$C_3H_6NO_2^+$	88.0399
Arginine (R)	7	$C_4H_{10}N_3^+$	100.0876
Valine (V) Arginine (R)	8	$C_4H_{10}N_3^+$	72.0813
Asparagine (N)	9	$C_4H_4NO_2^+$	98.0242
Tryptophan (W)	10	$C_4H_5O^+$	69.0340
Proline (P)	11	$C_4H_6N^+$	68.0501
Glutamine (Q) Glutamic Acid (E) Lysine (K)	12	$C_4H_6NO^+$	84.0449
Proline (P)	13	$C_4H_8N^+$	70.0293
Methionine (M) Glutamic Acid (E)	14	$C_4H_8NO_2^+$	102.0600
Leucine (L) Lysine (K)	15	$C_5H_{10}N^+$	84.0813
Arginine (R)	16	$C_5H_{11}N_4^+$	127.0932
Isoleucine (I) Leucine (L)	17	$C_5H_{12}N^+$	86.0970
Arginine (R)	18	$C_5H_{13}N_4^+$	129.1140
Valine (V) Glutamic Acid (E)	19	$C_5H_7O^+$	83.0497
Arginine (R)	21	$C_6H_{10}NO^+$	112.0762
Tyrosine (Y)	22	$C_7H_7O^+$	107.0497
Phenylalanine (F)	23	$C_8H_{10}N^+$	120.0813
Tyrosine (Y)	24	$C_8H_{10}NO^+$	136.0777
Tryptophan (W)	25	$C_9H_8N^+$	130.0640
Asparagine (N)	26	CH_2NO^+	44.0136
Arginine (R)	27	$CH_4N_2^+$	44.0375
Arginine (R)	28	$CH_5N_3^+$	59.0483

3.4.2 Data Processing using PCA

Although ToF-SIMS has major benefits when analyzing biological systems such as proteins, there are also some drawbacks. One such obstacle is the challenge of interpretation in ToF-SIMS spectra of proteins. Protein spectra are a challenge due to the high abundance of low=mass (0-200 *m/z*) fragments and the relative absence of high-mass protein fragments that might be unique to a biomolecule.[47] The amino acids that are part of the protein as a whole do display characteristic fragmentation patterns and have been studied in some depth.[48,6] These characteristic amino-acid fragments can be used to identify a particular amino acid, but not to identify a specific protein due to the fact that all large proteins consist of the same 20 amino acids. We postulate that by evaluation of the secondary-ion fragmentation patterns of amino acids associated with a particular protein bound to a surface in a particular manner, and knowledge of the binding or adsorption state of each protein, the patterns of peak intensities can be indicative of the orientation of the protein bound to the surface. For example, in the covalent reaction scheme used herein, the protein will prefer a particular orientation on the surface, resulting in similar patterns of secondary-ion fragmentation. For the non-specifically adsorbed protein, the protein will not likely have the same uniformity of orientation on the surface since the non-specific physical adsorption of proteins is driven largely by hydrophobic interactions.[4] The patterns of secondary-ion fragmentation of this protein's amino acids will likely differ from those of the covalently bound proteins. The ability of PCA to find such patterns in the differences between samples makes it ideally suited to the intended task here.

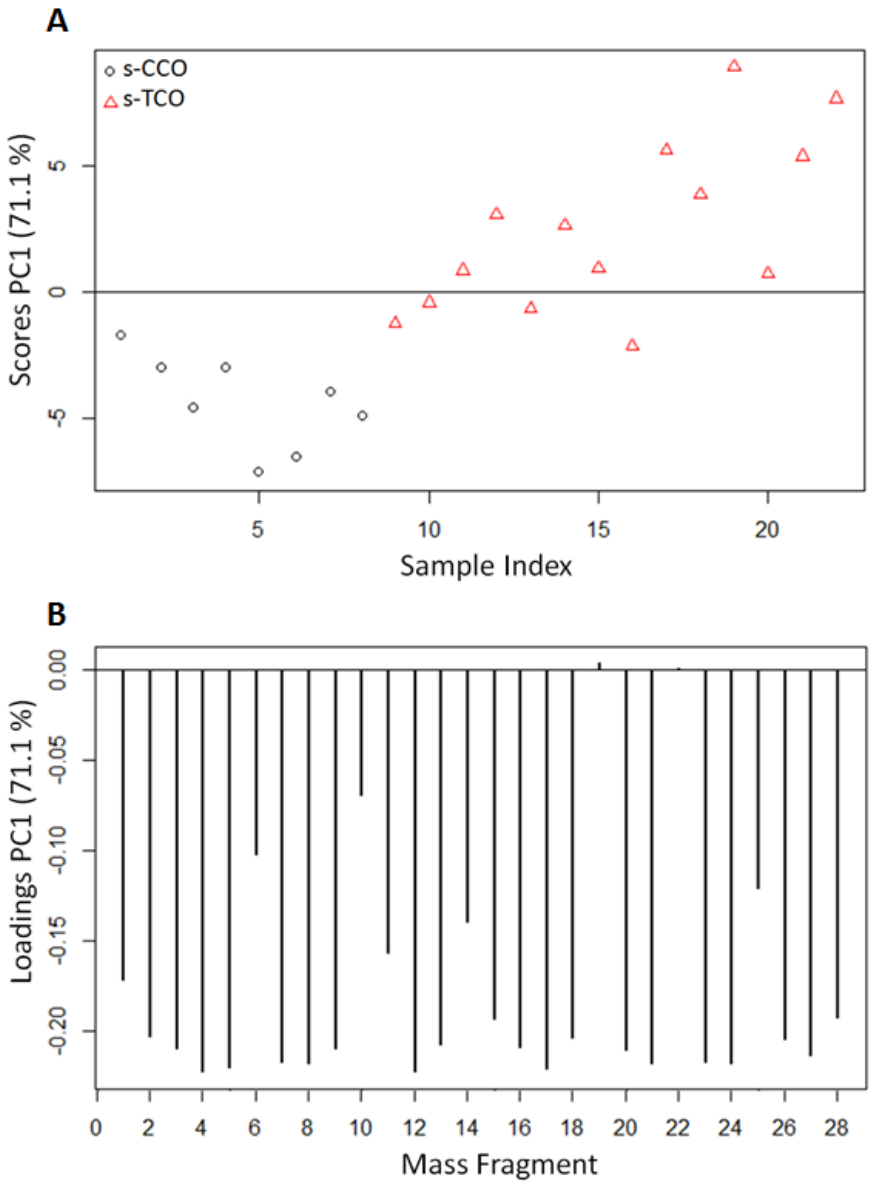

Figure 3.14 (A): PC1 scores for each sample from a PCA analysis of ToF-SIMS data for reaction of GFP-Tet with s-CCO (black "o" data symbols) and s-TCO (red "Δ" data symbols). (B): Loadings of PC1 mapped to the 28 possible mass fragments, showing which amino acid fragments are most responsible for the observed differences between samples for this new variable (PC1).

Table 3.5 is a complied list of identified amino acid fragments used to construct a data set for PCA analysis. The mass fragment index within Table 3.5 is merely a naming method for the amino-acid fragments and is used in all loadings plots herein (Figure 3.14 and Figure 3.15). The PC1 scores and loadings plots for the GFP-Tet protein on s-TCO (reactive) and s-CCO (unreactive) substrates are displayed in Figure 3.14. The PC1 scores plot accounts for about 71.1% of the variance in the data between samples (differences in ratios of secondary ion fragmentation peaks of amino acids). There is an observable separation between the covalently bound GFP-Tet (s-TCO-modified substrate) from that of the non-specifically adsorbed GFP-Tet (s-CCO-modified substrate). This separation signifies a difference in the ratio of amino acids that are ionized on the surface during ToF-SIMS analysis. Based on PC1 loadings plot (Figure 3.14) the majority of amino acid fragmentation peaks have a negative loading, the two most intense being $C_2H_6NO^+$ (serine) and $C_4H_6NO^+$ (glutamine, glutamic acid, and lysine), while there are two with positive loadings, $C_5H_7O^+$ (valine and glutamic acid) and $C_7H_7O^+$ (tyrosine). The direction and intensity of the amino acids in the loadings plot then correlates to the samples position on PC1 scores plot. The position of the covalently bound GFP-Tet within PC1 scores indicates higher, positively correlated, ratios of the three positively loaded amino acids. The position of the non-specifically adsorbed GFP-Tet within PC1 scores then indicate higher ratios of the two negatively loaded amino acids. This is one indication that the orientation of the covalently bound GFP-Tet allows for a higher ratio of $C_5H_7O^+$ and $C_7H_7O^+$ while the non-specifically adsorbed GFP-Tet allow for a higher ratio of $C_2H_6NO^+$ and $C_4H_6NO^+$.

Figure 3.15 displays the cross-plot of PC1 (*x*-axis) versus PC2 (*y*-axis) with the loadings for PC2 beneath. Evaluating PC2 scores there is a tight grouping of the non-specifically adsorbed GFP-Tet as well as a separation of s-TCO from the s-CCO bound protein. From the position of the non-specifically adsorbed GFP-Tet it can be noted that the fragmentation ratios of amino acids tend to group similar across PC1 as well as PC2 while that of the covalently bound protein does not. The importance of this is that the s-CCO control group only adsorbs proteins non-specifically, which means the hydrophobic domains that allow for the adsorption of the protein to the substrate surface is the dominant pathway leading to adsorption which, in this case, causes a consistent orientation of the protein to the surface.[49] The factors that influence the binding of the protein in the s-TCO-modified system include both the site-specific binding area of the GFP-Tet as well as hydrophobic interaction of the protein with the surface. Because of the size of the protein in relation to the single site specific binding area and the fact that there are competing hydrophobic domains both processes of covalent binding as well as adsorption in the s-TCO system are taking place. The positioning of the GFP-Tet bound to s-TCO in the PC2 scores plot shows the influence of the hydrophobic interactions dominating adsorption for some samples where covalent binding dominates in others.

Principal component analysis of characteristic secondary ion amino acid peaks showed that there is a difference in the low mass fragmentation patterns of those ions. The difference in fragmentation patterns is attributed to the availability of amino acids within the protein being analyzed, and as such the orientation of the protein bound to the surface.

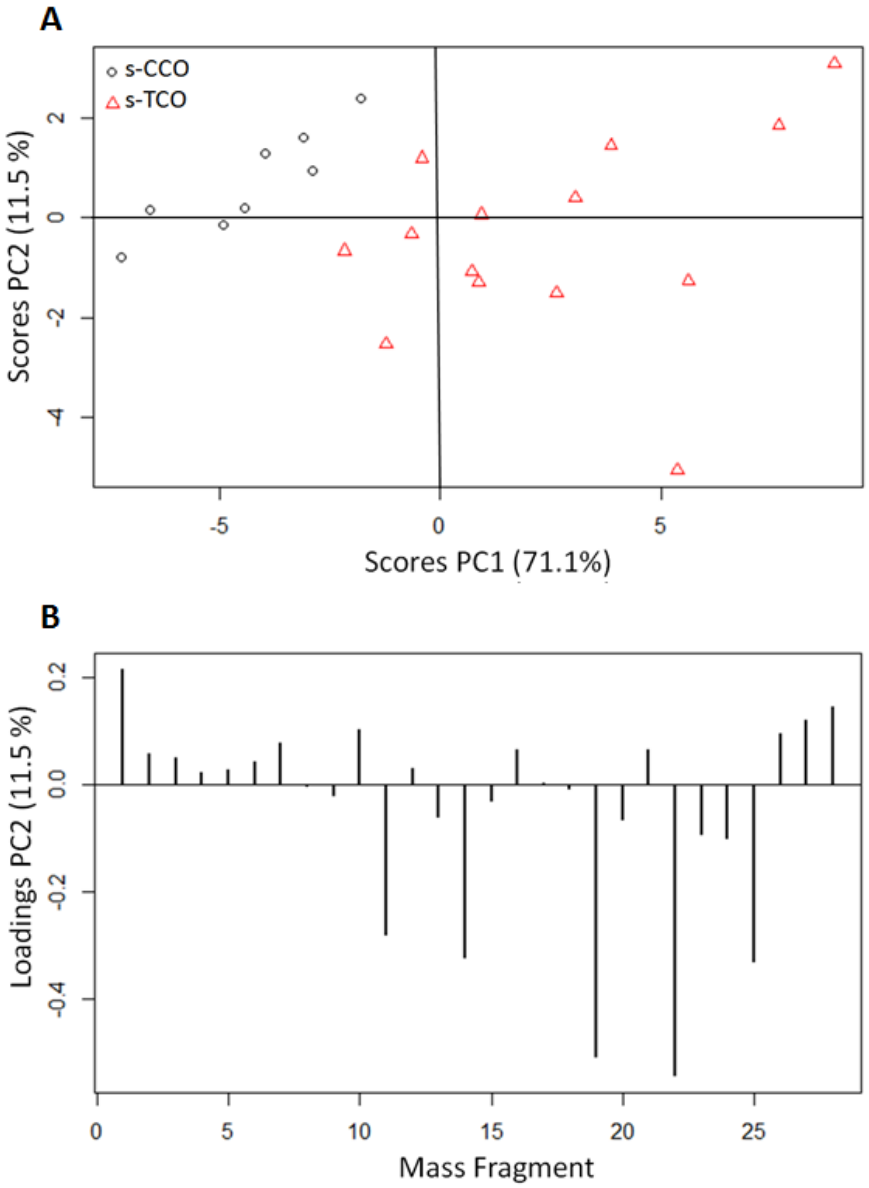

Figure 3.15 (A): PC1 vs. PC2 scores plot from a PCA analysis of ToF-SIMS data for reaction of GFP-Tet with s-CCO (black "o" data symbols) and s-TCO (red "Δ" data symbols). (B): Loadings of PC2 mapped to the 28 possible mass fragments, showing which amino acid fragments are most responsible for the observed differences between samples for this new variable (PC2).

Chapter 4

CONCLUSIONS

Several techniques within the scope of this work were used to verify the successful functionalization and binding of proteins to a solid support. Statistical comparison of contact angle measurements before and after APTMS modification were consistent with contact-angle measurements observed in previous unpublished work and confirmed the successful functionalization of amine-terminated silanes. Both solution-phase and vapor-phase methods used for APTMS-modification were compared. The solution-phase silanization method resulted in a more hydrophobic surface that indicated a higher density of accessible amine groups. ToF-SIMS analysis of the APTMS-modified surfaces further confirmed the successful functionalization through evaluation of unique secondary ions.

ToF-SIMS molecular imaging displayed successful micro-contact patterning of cyclooctene moieties and covalent or non-specific adsorption of a site-specifically modified tetrazine-protein within the functionalized lanes. Spectrum analysis of secondary ion fragments characteristic to amino acids further confirmed adsorption of GFP-Tet within micro-contacted lanes. By combining ToF-SIMS spectrum and fluorescent microscopy imaging functionalized proteins were confirmed to be more densely localized to the micro-contact patterned regions of the functionalized slides (s-TCO-modified or s-CCO-modified lanes). In addition, fluorescent microscopy showed the quenched fluorescence of GFP-Tet returning after binding of the Tetrazine to the s-TCO-modified substrate. The non-specifically adsorbed proteins in the s-CCO system

retained a smaller ratio of fluorescence between the functionalized and amine terminated lanes. The magnitude of quenched fluorescence in the s-CCO substrate indicated that the π system within the Tetrazine remained primarily unreacted resulting in the fluorescence of the GFP-Tet to remain quenched. The magnitude of difference in fluorescence intensity confirm covalent or non-specific adsorption of GFP and GFP-Tet to the surface.

Principal component analysis was utilized in conjunction with ToF-SIMS spectrum of characteristic amino acid fragments to evaluate the orientation of bound proteins on the s-TCO or s-CCO functionalized surface. Analysis of PC1 scores and loadings indicated a separation between the covalently and non-covalently bound proteins based on the availability of three amino acids. While PC1 showed a clear separation of covalently and non-covalently bound protein, PC2 did not. PC2 scores and loadings indicated that there were similarities between both systems. While covalent binding is preferential in the s-TCO-modified substrate and hindered in the s-CCO-modified substrate, non-specific binding is occurring on both surfaces. The similar non-specific binding of GFP or GFP-Tet results in the similarities of amino acid fragmentation ratios observed in PC2.

Future work for the functionalization of surfaces and ability to control the orientation of proteins to that surface will include procedures to control the amount of non-specifically adsorbed proteins to the surface. One possible route will be to combine poly(ethylene) glycol (PEG) architecture to the surface which has been proven to reduce non-specific protein adsorption.[50]

REFERENCES

(1) Rich, R. L.; Myszka, D. G. *J. Mol. Recognit.* **2008**, *21* (6), 355–400.

(2) Nakanishi, K.; Sakiyama, T.; Kumada, Y.; Imamura, K.; Imanaka, H. **2008**, 161–175.

(3) Jung, D. R.; Kapur, R.; Adams, T.; Giuliano, K. A.; Mrksich, M.; Craighead, H. G.; Taylor, D. L. *Topographical and Physicochemical Modification of Material Surface to Enable Patterning of Living Cells*; 2001; Vol. 21.

(4) Blawas, a. S.; Reichert, W. M. *Biomaterials* **1998**, *19* (7-9), 595–609.

(5) Castner, D. G.; Ratner, B. D. *Biomedical surface science: Foundations to frontiers*; 2002; Vol. 500.

(6) Wagner, M. S.; Horbett, T. A.; Castner, D. G. *Langmuir* **2003**, No. 16, 1708–1715.

(7) Wang, H.; Castner, D. G.; Ratner, B. D.; Jiang, S. *Langmuir* **2004**, *20* (15), 1877–1887.

(8) Henry, M.; Dupont-Gillain, C.; Bertrand, P. *Langmuir* **2003**, *19* (15), 6271–6276.

(9) Aoyagi, S.; Imai, R.; Sakai, K.; Kudo, M. *Biosens. Bioelectron.* **2003**, *18* (5-6), 791–795.

(10) Aoyagi, S.; Kudo, M. *Sensors Actuators B Chem.* **2005**, *108* (1-2), 708–712.

(11) Horbett, T. A. *Colloids Surfaces B Biointerfaces* **1994**, *2* (1-3), 225–240.

(12) Lee, Y.; Mrksich, M.; Lee, Y.; Mrksich, M. **2002**, *20* (12), 14–19.

(13) Houseman, B. T.; Mrksich, M. **2002**, *9* (02), 443–454.

(14) Wiley, J. **2009**, No. January, 393–397.

(15) Blackman, M. L.; Royzen, M.; Fox, J. M. *J. Am. Chem. Soc.* **2008**, *130* (41), 13518–13519.

(16) Seitchik, J. L.; Peeler, J. C.; Taylor, M. T.; Blackman, M. L.; Rhoads, T. W.; Cooley, R. B.; Refakis, C.; Fox, J. M.; Mehl, R. a. *J. Am. Chem. Soc.* **2012**, *134* (6), 2898–2901.

(17) Machida, T.; Lang, K.; Xue, L.; Chin, J. W.; Winssinger, N. *Bioconjug. Chem.* **2015**, 150421150845002.

(18) Devaraj, N. K.; Weissleder, R. *Society* **2011**, *44* (9).

(19) Ahern, P. *Time - of - Flight Secondary Ion Mass Spectrometry (ToF - SIMS)*; Glasnevin, Ireland, 2013.

(20) Wagner, M. S.; Castner, D. G. **2001**, No. 30, 4649–4660.

(21) Hagenhoff, B. *Mikrochim. Acta* **2000**, *132*, 259–271.

(22) Van Vaeck, L.; Adriaens, a; Gijbels, R. *Mass Spectrom. Rev.* **1999**, *18* (1), 1–47.

(23) Wagner, M. S.; McArthur, S. L.; Shen, M.; Horbett, T. A.; Castner, D. G. *J. Biomater. Sci. Polym. Ed.* **2002**, *13* (4), 407–428.

(24) Marletta, G.; Catalan, S. M.; Pignataro, S.; Chimiche, S.; Catania, U.; Dona, W. a. **1990**, *16*, 407–411.

(25) Lhoest, J. B.; Wagner, M. S.; Tidwell, C. D.; Castner, D. G. *J. Biomed. Mater. Res.* **2001**, *57* (3), 432–440.

(26) Wagner, M. S.; Castner, D. G. *Appl. Surf. Sci.* **2004**, *231-232*, 366–376.

(27) Zhang, Z.; Yoo, R.; Wells, M.; Beebe, T. P.; Biran, R.; Tresco, P. *Biomaterials* **2005**, *26* (1), 47–61.

(28) Graham, D. J.; Wagner, M. S.; Castner, D. G. *Appl. Surf. Sci.* **2006**, *252* (19), 6860–6868.

(29) Longsdorf, K. M. A novel strategy for biomolecular presentation on surfaces using tetrazine ligation, 2011.

(30) Balachander, N.; Sukenik, C. N. *Langmuir* **1990**, *6* (11), 1621–1627.

(31) Liebmann-Vinson, A.; Lander, L. M.; Foster, M. D.; Brittain, W. J.; Vogler, E. A.; Majkrzak, C. F.; Satija, S. *Langmuir* **1996**, *12* (9), 2256–2262.

(32) Heise, A.; Menzel, H.; Yim, H.; Foster, M. D.; Wieringa, R. H.; Schouten, A. J.

1997, *7463* (9), 723–728.

(33) Mourougou-Candoni, N.; Thibaudau, F. *J. Phys. Chem. B* **2009**, *113* (39), 13026–13034.

(34) Fiorilli, S.; Rivolo, P.; Descrovi, E.; Ricciardi, C.; Pasquardini, L.; Lunelli, L.; Vanzetti, L.; Pederzolli, C.; Onida, B.; Garrone, E. *J. Colloid Interface Sci.* **2008**, *321* (1), 235–241.

(35) Kurth, D. G.; Bein, T. *Langmuir* **1993**, *9* (11), 2965–2973.

(36) Wang, W.; Vaughn, M. W. *Scanning* **2008**, *30* (2), 65–77.

(37) Halliwell, C. M.; Cass, a E. *Anal. Chem.* **2001**, *73* (11), 2476–2483.

(38) Gotliv, B.-A.; Robach, J. S.; Veis, A. *J. Struct. Biol.* **2006**, *156* (2), 320–333.

(39) Awsiuk, K.; Budkowski, a; Psarouli, a; Petrou, P.; Bernasik, a; Kakabakos, S.; Rysz, J.; Raptis, I. *Colloids Surf. B. Biointerfaces* **2013**, *110*, 217–224.

(40) Kim, Y.-P.; Hong, M.-Y.; Kim, J.; Oh, E.; Shon, H. K.; Moon, D. W.; Kim, H.-S.; Lee, T. G. *Anal. Chem.* **2007**, *79* (4), 1377–1385.

(41) Kim, Y.-P.; Hong, M.-Y.; Shon, H. K.; Moon, D. W.; Kim, H.-S.; Lee, T. G. *Appl. Surf. Sci.* **2006**, *252* (19), 6801–6804.

(42) Aoyagi, S.; Gilmore, I. S.; Mihara, I.; Seah, M. P.; Fletcher, I. W. *Rapid Commun. Mass Spectrom.* **2012**, *26* (23), 2815–2821.

(43) Ma, H.; Hyun, J.; Zhang, Z.; Beebe, T. P.; Chilkoti, a. *Adv. Funct. Mater.* **2005**, *15* (4), 529–540.

(44) Taylor, M. T.; Blackman, M. L.; Dmitrenko, O.; Fox, J. M. **2011**, 9646–9649.

(45) Liang, Y.; Mackey, J. L.; Lopez, S. a; Liu, F.; Houk, K. N. *J. Am. Chem. Soc.* **2012**, *134* (43), 17904–17907.

(46) Devaraj, N. K.; Upadhyay, R.; Haun, J. B.; Hilderbrand, S. a; Weissleder, R. *Angew. Chem. Int. Ed. Engl.* **2009**, *48* (38), 7013–7016.

(47) Muramoto, S.; Graham, D. J.; Wagner, M. S.; Lee, T. G.; Moon, D. W.; Castner, D. G. *J. Phys. Chem. C* **2011**, *115* (49), 24247–24255.

(48) Wagner, M. S.; Horbett, T. A.; Castner, D. G. *Biomaterials* **2003**, *24* (11), 1897–1908.

(49) Ruggiero, C.; Mantelli, M.; Curtis, A.; Rolfe, P. *Cell Biochem. Biophys.* **2005**, *43* (3), 407–417.

(50) Xia, N.; Hu, Y.; Grainger, D. W.; Castner, D. G. *Synthesis (Stuttg).* **2002**, No. 23, 3255–3262.